Energy Conversion and Management 175 (2018) 67–85

Contents lists available at ScienceDirect

Energy Conversion and Management

journal homepage: www.elsevier.com/locate/enconman

Technoeconomic modelling and optimisation of solar combined heat and power systems based on flat-box PVT collectors for domestic applications

María Herrando[a,b], Alba Ramos[a,c], James Freeman[a], Ignacio Zabalza[b], Christos N. Markides[a,*]

[a] Clean Energy Processes (CEP) Laboratory, Department of Chemical Engineering, Imperial College London, London, UK
[b] School of Engineering and Architecture, University of Zaragoza, Zaragoza, Spain
[c] Solar Energy Institute, Technical University of Madrid, Spain

ARTICLE INFO

Keywords:
Solar energy
Hybrid PVT collector
Flat-box structure
Combined heat and power
Technoeconomic modelling

ABSTRACT

We investigate solar combined heat and power (S-CHP) systems based on hybrid photovoltaic-thermal (PVT) collectors for the simultaneous provision of domestic hot water (DHW), space heating (SH) and power to single-family homes. The systems include PVT collectors with a polycarbonate flat-box structure design, a water storage tank, an auxiliary heater and a battery storage subsystem. A methodology is developed for modelling the energetic and economic performance of such PVT-based S-CHP systems, which is used to optimally size and operate systems for covering the energy demands of single-family reference households at three selected locations: Athens (Greece), London (UK) and Zaragoza (Spain). The results show that optimised systems are capable of covering ~65% of the annual household electricity demands in Athens, London and Zaragoza when employing 14.0, 17.0 and 12.4 m^2 collector array areas respectively, while also covering a significant fraction of the thermal energy demands in Athens (~60%) and Zaragoza (~45%); even in London, almost 30% of the reference household's thermal demand is covered by such a system. A corresponding economic analysis reveals that, despite the suitability of Athens' weather conditions for implementing such solar-energy systems, the payback time (PBT) of the optimised S-CHP system in Athens is 15.6 years in contrast to the 11.6 years predicted for Zaragoza, due to the lower electricity prices in Greece. On the other hand, the high carbon emission factor of the electricity grid in Greece makes these systems particularly promising at this location. Specifically, the investigated systems have the potential to displace 3.87, 1.65 and 1.54 tons of CO_2 per year in Athens, London and Zaragoza, when substituting the conventional means for household energy provision (i.e. grid electricity and gas-fired boilers). Furthermore, it is demonstrated that the optimised systems outperform benchmark equivalent systems comprising conventional sheet-and-tube PVT collectors in all studied cases, by covering similar or slightly (up to 3%) higher fractions of the household electrical and thermal demands with 9–11% lower PBTs, and that PV-only solutions displace 3.56, 1.21, 1.22 tCO_2/year (up to ~20–25% lower) for the same area. Overall, the results suggest that the newly proposed polymeric flat-box PVT collector designs are an improved economic proposition over their conventional equivalents, but that the cost of this technology still remains high relative to PV and that if decarbonisation is a desirable goal, especially in high population-density regions with space restrictions, it is important to consider how to promote this technology.

1. Introduction

The utilisation of solar energy is a key enabler of the transition to a clean and sustainable energy future [1,2]. Despite the widespread acceptance, significant market growth and deployment of photovoltaic (PV) systems, and the wide range of products available on the market, some challenges remain that hinder their potential. Of particular interest are the limited conversion efficiencies experienced at elevated operation temperatures and the greater thermal cycling experienced (passively) in response to external weather conditions, both of which also act to damage the PV cells. This has motivated important research into cooling techniques for the thermal regulation of PV modules [3], which has led to the proposal of hybrid photovoltaic-thermal (PVT) collectors, comprising a PV module typically laminated on top of a thermal absorber for heat removal, that are therefore capable of generating both electrical and thermal outputs from the same collector area [4]. Similarly to conventional PV and solar-thermal (ST) systems, PVT systems are a means of moving energy generation closer to the point of

* Corresponding author.
E-mail address: c.markides@imperial.ac.uk (C.N. Markides).

https://doi.org/10.1016/j.enconman.2018.07.045
Received 28 March 2018; Received in revised form 10 July 2018; Accepted 13 July 2018

Nomenclature

Abbreviations

BSD	(monthly) battery self-discharge rate
DHW	domestic hot water
FIT	feed-in tariff
FS	fuel saving
IEA	International Energy Agency
pc-Si	poly-crystalline silicon
PC	polycarbonate
PBT	payback time
PV	photovoltaic
PVT	photovoltaic-thermal system
PVT-w	photovoltaic-thermal water system
RHI	renewable heat incentive
SEER	seasonal energy efficiency ratio
SH	space heating
ST	solar thermal
TIC	transparent insulating cover
LCC	life cycle cost
LPC	levelised production cost
NPV	net present value
S-CHP	solar combined heat and power
SOC	state of charge
UFH	(radiant) underfloor heating

Symbols

A_c	PVT collector aperture area (m^2)
A_{coil}	coil heat transfer area (m^2)
A_{cT}	total PVT collectors area (m^2)
$A_{surf,t,n}$	surface area of the tank at node n (m^2)
c_p	specific heat capacity (J/kg·K)
C	battery capacity (Ah)
C_{conv}	annual household running costs (€)
c_e	electricity price (€/kWh)
c_{ng}	natural gas price (€/kWh)
C_0	investment costs (€)
$C_{C/D}$	battery charge/discharge capacity (Ah)
$C_{O\&M}$	operation and maintenance (O&M) costs (€/yr)
$C_{S\text{-}CHP}$	annual running costs of household with S-CHP system (€/yr)
C_T	battery energy capacity (Wh)
d	discount rate (%)
D_h	hydraulic diameter (m)
D_t	tank diameter (m)
E	energy (Wh)
f	friction factor (–)
H	height (m)
i	time step (–)
i_F	fuel inflation rate (%)
$I_{C/D}$	actual charge and discharge current (A)
$I_{C0/D0}$	available charge/discharge current (A)
$I_{Cmax/Dmax}$	maximum allowed charge and discharge current (A)
I_T	total solar irradiance per meter square (W/m^2)
L_e	levelised cost (€/yr)
m_t	storage tank water mass (kg)
$\dot{m}$	mass flow-rate (kg/s)
$\dot{m}_c$	mass flow-rate per PVT collector (kg/s)
$\dot{m}_{cT}$	total mass flow-rate through the PVT collectors (kg/s)
n	node (–)
n	system lifetime (yr)
N	total number of PVT collectors (–)
N_n	total number of tank nodes (–)
P	power (W)
Q	heat flow (W)
Re	Reynolds number (–)
S	absorbed solar irradiance (W/m^2)
T	temperature (K)
U	overall heat transfer coefficient (W/m^2 K)
$(UA)_t$	thermal conductance of storage tank heat exchanger (W/K)
V_t	storage tank volume (L)
V_B	battery voltage (V)
V_p	PVT collector flow-rate (L/h)

Greek

β	PVT collector tilt angle (°)
λ_{eff}	effective vertical thermal conductivity in storage tank (W/m·K)
ΔC	change in battery capacity (Ah)
Δp	total pressure drop through S-CHP system (Pa)
Δt	time step (s)
ΔT	temperature difference (–)
ε	heat exchanger effectiveness (–)
η	efficiency (%)
ρ	density (kg/m^3)

Subscripts

a	ambient
aux	auxiliary heat
bat	batteries
BC	battery charge
BD	battery discharge
c	PVT collector
cc	charge controller
cond	conduction
conv	conventional means
cov	covered
ct	from PVT collector to storage tank
D	household demand
DT	total household demand
dump	heat rejected to the atmosphere
e	electrical
exp	surplus electricity exported to the grid
gen	generated
grid	electricity imported from the grid
hh	half-hourly
in	inlet
int	surroundings of the storage tank
inv	inverter
loss	losses
net	net energy/power in the household
out	outlet
o	optical
out	PVT collector outlet
PVT	energy/power generated by the PVT collectors
r	reduced
t	water storage tank
th	thermal
T	total
TDeq	total household demand converted to “equivalent” electricity
Teeq	total “equivalent” electricity
Tpe	total primary energy
w	water
win	mains water entering the water storage tank

use, and thereby of reducing the demands on costly energy distribution infrastructure [5]. This makes these systems particularly promising for distributed deployment in domestic applications, which are at the focus of this work. Thus, a solar combined heat and power (S-CHP) system based on hybrid PVT collectors is hereby proposed, studied and optimised from both energetic and economic perspectives. This study extends earlier work that considered PV-only systems [6,7] and/or separate S-CHP systems based on ST collectors [8] for heat and power provision to buildings, including such systems based on low-temperature thermodynamic power cycles [9–12], as well as some limited attempts to consider PVT-based S-CHP systems [13].

The most widely studied absorber-exchanger design in PVT collectors is that of parallel copper tubes (sheet-and-tube) with water or water-glycol mixtures as the heat transfer fluid [14–18], which is also the one used most commonly in commercially-available collectors [19]. In this design, the amount of heat that can be extracted, and thus the overall efficiency that can be achieved, depend on the collector fin efficiency and the tube bonding quality [20]. Consequently, several investigators have made significant efforts to optimise the design of these collectors by paying attention to these design aspects [16,17], while others have proposed an alternative flat-box structure with square or rectangular channels in order to significantly increase the heat transfer area between the absorber plate and the cooling fluid [14,20–25]. Some of these studies [14,20,25] have considered extruded aluminium alloy as the absorber-exchanger material, while others [21,23,24] have proposed polycarbonate (PC) as the material of choice in order to lower the cost and weight of the collector. The work presented here focuses on a novel PVT water collector designed and modelled in previous research [26], based on a PC 3×2 mm flat-box structure. Previous research undertaken by the authors [26] concluded that this absorber-exchanger design can achieve a 4% higher optical efficiency and a 15% lower heat loss coefficient, leading also to a 9% reduction in weight and a 21% reduction in investment cost compared to a commercial PVT collector based on a copper sheet-and-tube arrangement.

A number of approaches have been used to estimate the operational characteristics, performance and economics of PVT systems [18,27–30]. Almost all previous studies were based in relatively low-latitude regions with a substantial solar resource, while previous R&D reviews [31] concluded that further work should focus on long term (seasonal, annual) analyses of system performance considering the influence of weather conditions. In this respect, the present research explores the potential of PVT-based S-CHP systems in three different European climates for comparison purposes, including the United Kingdom (UK), which is representative of cooler northern climates with lower levels of solar irradiation. Significantly different results are expected at different locations, not only due to the different environmental conditions, but also due to the different household energy demands, electricity and gas prices, policies and incentives, etc.

The electricity and heat consumed by a household are both strongly dependent on occupant behaviour. Therefore, in order to design and size appropriately an S-CHP system for domestic heating, including space heating (SH) and domestic hot water (DHW), as well as power provision, it is necessary to know these energy profiles [32]. Research in this field has typically considered monthly household energy demand profiles based on degree-days [33], or estimated daily profiles [18,27]. Other studies that did model the building energy-demand profiles, did not include full user profiles and internal gains [34]. More recently, some authors have begun to consider the building energy demands in detail, in particular for the analysis of solar polygeneration systems installed in university buildings [35] and offices [36]. Such efforts include detailed household energy models that can account not only for the specific weather conditions, but also for the transient occupancy profiles and operation schedules of the various household energy consuming devices (i.e. HVAC systems, electric appliances, etc.), thereby providing useful estimates of the household energy demand profiles. In this present research, reference homes have been modelled in EnergyPlus [37], including occupancy profiles and operation schedules, leading to household energy demand estimates at half-hourly time-steps over a whole year. Previous studies [38,39] that considered DHW provision concluded that the use of a stratified storage tank enhances the thermal performance of the PVT systems. However, the provision of space heating by radiant underfloor heating (UFH) with the thermal output of PVT water collectors has not been investigated.

The two main options for increasing the electrical self-consumption of residential S-CHP installations are energy storage and demand-side management (DSM), which can be implemented either as part of separate or combined strategies [40,42]. This research considers energy storage, both thermally which is standard in such systems, and also electrically in an attempt to reduce the interaction of the investigated systems with the electrical grid, whose availability/reliability comes at an external cost that is rarely accounted for in similar studies. One of the most common types of battery technology used in PV systems is the lead-acid battery due to its maturity and low-cost, with lithium-ion batteries recently gaining market share although their costs still remain higher [7,43,44]. In this work we focus on the former.

When modelling PVT systems, the temporal resolution chosen for the simulations has been shown to significantly affect system performance predictions [40,41]. A low resolution can lead to an overestimation of self-consumption, because any mismatch between the instantaneous generation and the load can be smoothed out, depending on how the data is aggregated or downsampled. In Ref. [40], it was concluded that half-hourly data is sufficient for the modelling of an individual building especially in order to capture the behaviour of load profiles during peak power consumption. Therefore, this research considers half-hourly time-steps for the S-CHP system simulations.

In Section 2, we present the modelling methodology and related assumptions that were used in its development, including details of the PVT-based S-CHP system model and parameters, the reference single-family houses modelled in EnergyPlus, the economic analysis undertaken and the economic and environmental parameters. Section 3 contains the main results and an associated discussion, including the selection of the key performance indicators for system sizing, the technoeconomic optimisation of the S-CHP system, the PVT collector operation optimisation, daily analysis and comparison of the optimised S-CHP systems in the different locations. Finally, the main conclusions from this work are summarised in Section 4.

2. Methodology and model definition

A quasi-steady state model of S-CHP systems has been developed in software Engineering Equation Solver (EES) [45], as an extension to a model developed in previous research [46], with the aim of assessing the technoeconomic performance of such systems, in particular when featuring polycarbonate flat-box PVT collector designs and electrical energy storage. System operation and performance are also compared to those of equivalent benchmark systems comprising commercial sheet-and-tube PVT collectors. Reference households in different regions are modelled through transient simulations in EnergyPlus [37] to estimate their energy demands in half-hourly steps throughout the year. Together with the weather conditions that are representative of the corresponding geographical locations of these households, the energy demands are used as inputs to the S-CHP system model in EES that simulates system performance in half-hourly time-steps. Key economic characteristics of S-CHP systems, including their capital (investment), running (electricity and natural gas) and operation/maintenance (O&M) costs, are also included in the model. The outputs returned by the model at each half-hourly time-step include the temperatures of the different layers of the PVT collector, the collector water outlet temperature, the water temperatures at each node in the storage tank, the state of charge (*SOC*) of the batteries, the electrical and thermal energy generated by the complete S-CHP system, the electrical and thermal energy demands of the household covered by the system, the energy,

cost and CO_2 emissions savings, the levelised production cost (*LPC*) and the payback time (*PBT*) of the system. The methodological approach is summarised with the help of a block diagram in Fig. 1.

2.1. S-CHP system model

The complete S-CHP model developed this work for the provision of heating (DHW and SH) and power to domestic users is shown in Fig. 2. The core components of this system are: the PVT collector array (Component 1), a pumped water closed-loop circulation loop that connects the PVT collector with the storage tank through an internal heat exchanger (Components 2 and 3), a stratified hot water storage tank (Component 4), an auxiliary heater (Component 6), and electrical storage provided by a number of lead-acid battery units connected to the PVT collectors and to the grid (Component 8). The energy demand breakdown of a reference house modelled in EnergyPlus is integrated as an input to the model together with the weather conditions (ambient temperature and solar irradiance) also taken from EnergyPlus (see Section 2.2). Most of the S-CHP system component parameters can be varied in the model, including: the PVT design (geometry, materials), the PVT collector flow-rate, the number of PVT collectors, the water storage tank volume, and the size and key features of the batteries.

The S-CHP system model was developed under the following assumptions: (i) the incident solar irradiance is absorbed only by the collector [47], and the light absorption by the cover glass and the frame are negligible, (ii) the ambient temperature is uniform around the PVT collector [38,48], (iii) solar irradiance is uniform on the collector surface, (iv) the temperature dependence of all relevant solid-component material properties can be neglected [49], (v) the water mass flow-rate is distributed uniformly between all riser tubes [38,50], (vi) free convection in the riser tubes is negligible, (vii) all radiative heat exchanges between the sides of the solar collectors' channels can be neglected [17,38,51,52], and (viii) the pipes connecting the PVT collectors to the water storage tank are well insulated, such that there are no heat losses to the environment [38].

2.1.1. PVT collector

This study considers a new flat-box PVT collector design and compares this to an equivalent commercially available sheet-and-tube collector, namely the ECOMESH PVT collector by company Endef Engineering [53]. The two main components of the flat-box PVT collector are the PV module and thermal absorber. As in previous work by the same authors [19] and similar modelling attempts [16,48], a set of energy conservation equations are written that describe the heat fluxes and temperatures through all layers of the collector. The equations are applied separately to each layer of the collector in order to identify the average absorber plate temperature, and to uncover the distribution of the average temperatures and energy flows through all separate component layers that comprise the collector [52,54]. The main heat transfer mechanisms that have been considered in this work for the different collector layers are shown in Fig. 3. Full details of the collector model can be found in Ref. [26].

The model contains the governing equations of the PVT collector detailed in previous work [26], based on the ASHRAE method [55], which includes parameters describing the PVT geometry (such as fin efficiency, F, heat removal factor, F_R, overall heat loss coefficient, U_L, etc.), adapted to the flat-box structure.

The aperture area and electrical characteristics of the polymeric flat-box PVT collector have been defined to be equal to those of the equivalent benchmark commercial sheet-and-tube PVT collector [53], i.e. 1.55 m^2 aperture area, 240 W_p electrical power, 14.7% nominal PV module efficiency and −0.45 %/K PV temperature coefficient. Thus, the two collectors vary only in terms of their thermal performance, as follows (see Fig. 4):

Sheet-and-tube (S&T) PVT collector (benchmark):

$$\eta_{th} = 0.700 - 3.937 \cdot T_r - 0.0155 \cdot I_T \cdot T_r^2 \quad (1)$$

Polycarbonate (PC) 3 × 2 flat-box PVT collector:

$$\eta_{th} = 0.726 - 3.325 \cdot T_r - 0.0176 \cdot I_T \cdot T_r^2 \quad (2)$$

As mentioned above, detailed technical specifications of the modelled PVT collectors can be found in Ref. [26].

2.1.2. Stratified water storage tank

A one-dimensional (1-D) model is used for the hot water storage tank. The tank is assumed to consist of N_n fully mixed equal volume segments that divide the cylinder along its vertical axis. Each segment is represented by a node n, where $n = 1$ is the bottom segment and $n = N_n$ is the top one. In this study, based on the results obtained in previous research where an adequate stratification was achieved [39], 6 nodes are considered ($N_n = 6$). The total mass of fluid in the tank is assumed constant. For the stratification, a temperature gradient is preserved in the tank by ensuring that the hot water for DHW demand is supplied via a port at the top of the tank ($n = N_n$), while replacement cold water from mains (at T_{win}) is introduced at the bottom ($n = 1$). A (gas-fired) auxiliary heater of sufficient power is installed at the outlet port at the top of the tank ($n = N_n$), to raise the temperature up to a fixed supply temperature of 60 °C when required.

In the sizing calculation, the storage tank volume is varied through the variation of the ratio V_t/A_{cT}, where V_t is the tank volume in litres and A_{cT} is the total PVT collector area. According to the Ministry of Housing of the Spanish Government [56], for ST installations in households this range should be kept between $50 < V_t/A_{cT} < 180$ (in L/m^2). The size of the solar heat exchanger coil (Component 5 in Fig. 2) also varies with the tank size, through the variation of the tank height, H_t, such $A_{coil}/A_{cT} \geq 0.15$ [57] to ensure adequate heat transfer. This coil runs the full length of the tank, with the coil inlet port positioned at the top ($n = 6$) and the coil outlet port positioned at the bottom of the tank ($n = 1$).

To provide SH (via radiant underfloor heating, UFH), a second heat exchanger coil is located in the tank (Component 7 in Fig. 2), which

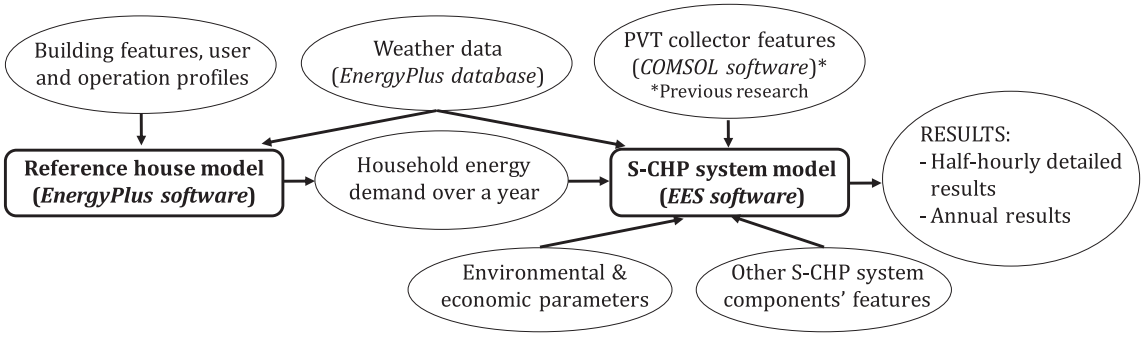

Fig. 1. Block diagram of the methodology followed in the present research.

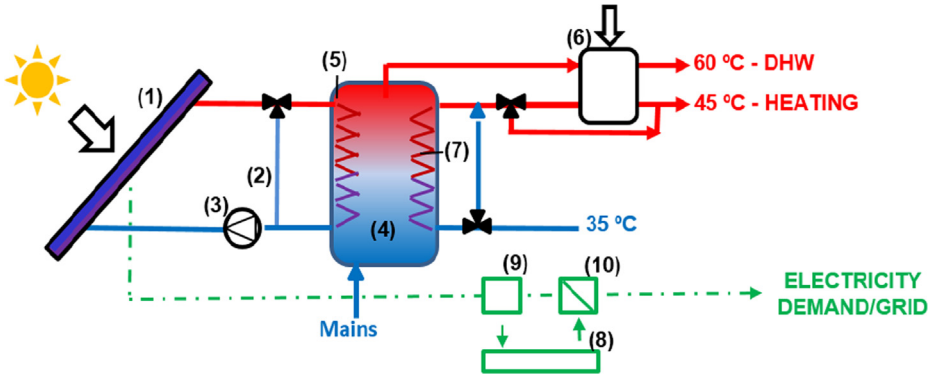

Fig. 2. Schematic diagram of the S-CHP PVT system: (1) PVT collector, (2) PVT bypass, (3) circulator pump, (4) stratified storage tank, (5) solar heat exchanger coil, (6) auxiliary heater, (7) space heating heat exchanger coil, (8) Lead-acid battery, (9) charge controller, (10) DC/AC inverter.

also varies with the tank size. Water flowing in a separate closed-loop circuit enters the heat exchanger coil at node $n = n_{SH,in}$ at the UFH return temperature of 35 °C, it is heated to a target supply temperature of 45 °C, and exits the tank at node $n = n_{SH,out}$. Again, a bypass is included to avoid sending fluid to the heat exchanger when the tank temperature is lower than 35 °C.

The hot water tank equations are based the Multiport Store model developed for TRNSYS, Type 340 [58]. The temperatures in each node of the tank are solved using the following explicit method, in which the temperature of the tank in each time-step (i) is used to evaluate the temperature of the tank in the subsequent time-step ($i + 1$). The energy balance for each node of the hot water cylinder is as follows:

$$T_{t,n}(i+1) = T_{t,n}(i) + \frac{Q_{DHW,n}(i) + Q_{SH,n}(i) + Q_{ct,n}(i) + Q_{cond,n}(i) + Q_{loss,n}(i) + Q_{dump,n}(i)}{m_{t,n} \cdot c_p} \cdot \Delta t, \quad (3)$$

where $T_{t,n}$ (i) and $T_{t,n}$ ($i + 1$) are the tank temperatures at node n at time-steps i and $i + 1$ respectively, $m_{t,n}$ is the amount of water (in kg) in each tank node, c_p is the specific heat capacity of water, Δt is the time-step duration (0.5 h in this case), and Q (i) are the heat flows that might take place in each node.

As mentioned above, the supply of DHW involves extracting water from the top of the tank and replacing this with mains water at the bottom. Therefore, at each node, the following heat transfer takes place:

$$Q_{DHW,n}(i) = \dot{m}_{DHW}(i) \cdot c_p \cdot (T_{t,n-1}(i) - T_{t,n}(i)), \quad (4)$$

where $\dot{m}_{DHW}(i)$ is the mass flow-rate of DHW demand which is a model input for each time-step. For the bottom node ($n = 1$), $T_{t,0} = T_{win}$.

According to Ref. [59], the most practical approach towards heat exchanger design for solar systems is based on the NTU-effectiveness (ε) method, so for each node containing a segment of the SH heat exchanger coil, the heat transferred from the coil fluid to the hot water in the tank is:

$$Q_{SH,n}(i) = \dot{m}_{SH}(i) \cdot c_p \cdot \varepsilon_{SH} \cdot (T_{coil,in,n}(i) - T_{t,n}(i)), \quad (5)$$

and the temperature of the fluid exiting the coil segment in one node, which becomes the temperature entering the next coil segment in the adjacent node, is:

$$T_{coil,out,n}(i) = T_{coil,in,n}(i) - \varepsilon_{SH} \cdot (T_{coil,in,n}(i) - T_{t,n}(i)). \quad (6)$$

The mass flow-rate of SH, $\dot{m}_{SH}(i)$, is provided to the model at each time-step. The heat exchanger effectiveness (ε_{SH}) can be predicted directly from the characteristics of the heat exchanger and the relevant flows [60].

Similarly, for each node containing a segment of the solar heat exchanger coil, the heat transferred from the fluid coming from the PVT collectors circulating to the hot water in the tank is:

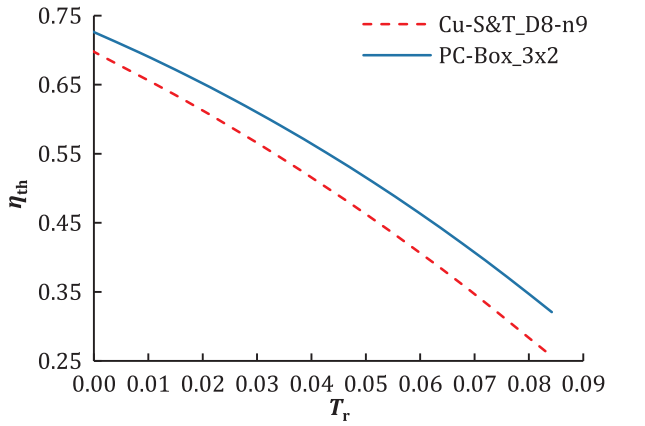

Fig. 4. Thermal efficiency curves of the benchmark S&T and PC flat-box PVT collectors based on Eqs. (1) and (2).

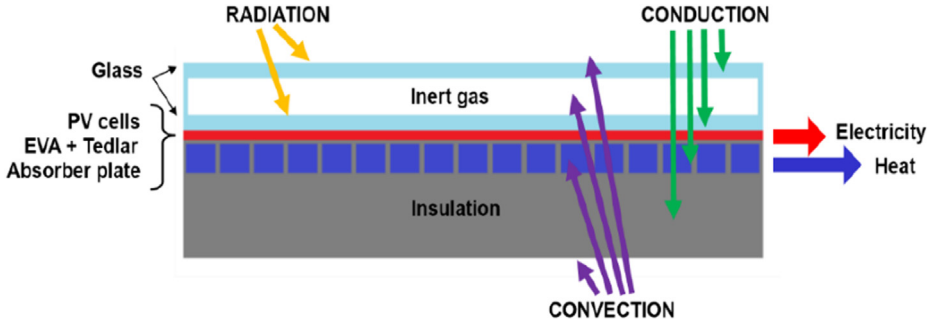

Fig. 3. Flat-box structure PVT collector design cross-section, showing the various collector layers and heat transfer mechanisms (not to scale) [26].

$$Q_{ct,n}(i) = \dot{m}_{cT}(i)\cdot c_p\cdot\varepsilon_{ct}\cdot(T_{coil,in,n}(i)-T_{t,n}(i)). \quad (7)$$

Thus, the temperature of the fluid exiting the coil segment in one node (from Eq. (6)) becomes the temperature of the fluid entering the next coil segment in the adjacent node. In this coil, the flow direction is downward with respect to the tank as shown in Fig. 2, such that $T_{coil,in,n} = T_{coil,out,n+1}$. Furthermore, the total mass flow-rate circulating through the PVT collector array, $\dot{m}_{cT}(i)$, in which a number of N PVT collectors are connected in parallel, is given by $\dot{m}_{cT}(i) = N\cdot\dot{m}_c(i)$, where $\dot{m}_c(i)$ the mass flow-rate per PVT collector. As before, the heat exchanger effectiveness (ε_{ct}) is calculated following Ref. [60], as part of the sizing exercise as it also varies with the tank volume (V_t).

The heat transfer by conduction between the tank nodes is described by the term $Q_{cond,n}$, expressed as:

$$Q_{cond,n}(i) = \frac{\lambda_{eff}\cdot\pi\cdot D_t^2}{4\cdot H_{t,n}}\bullet(T_{t,n+1}(i) + T_{t,n-1}(i)-2\cdot T_{t,n}(i)), \quad (8)$$

where λ_{eff} is the effective vertical thermal conductivity, D_t is the tank diameter and $H_{t,n}$ is the height of node n of the tank. A constant diameter (1 m) is considered such that the tank height varies accordingly to the tank volume. The effective vertical thermal conductivity is a lumped parameter that takes into account conduction in the water, the walls of the tank and the internal components such as the heat exchanger coils. A value of 1.85 W/(m K) is chosen, which is representative of a range of solar hot water cylinders [61].

The thermal energy loss to the internal environment through the tank walls is given by:

$$Q_{loss,n}(i) = U_t\cdot A_{surf,t,n}\cdot(T_{int}-T_{t,n}(i)), \quad (9)$$

where the indoor temperature surrounding the cylinder T_{int} is assumed constant at 20 °C, U_t is the overall tank heat loss coefficient taken to be 3 W/m^2 K [19,47,62], and $A_{surf,t,n}$ is the tank surface area at node n.

Finally, to avoid overheating in the tank, water is extracted from the top and replaced by cold mains water at the bottom when the temperature at the top of the tank is above 80 °C [63]. Then, the heat rejected, $Q_{dump,n}$, is calculated as if there was DHW demand, that is:

$$Q_{dump,n}(i) = \dot{m}_{dump}(i)\cdot c_p\cdot(T_{t,n-1}(i)-T_{t,n}(i)). \quad (10)$$

2.1.3. Rest of system

The model comprises an active closed loop system, composed by Components 1–3 and 5 in Fig. 2. In normal operation, the collector outlet flow enters the heat exchanger coil located inside the storage tank, heats the water in the tank, exits the tank and returns to the inlet of the solar collector to be heated again. A bypass valve is required to control the temperature of the cooling fluid leaving the collector and entering the tank, to ensure that this stream only heats (and does not cool) the water in the tank, as done in Refs. [19,77]. A differential temperature controller, widely used in ST systems, controls the valve position by comparing the temperature at the entrance of the heat exchanger coil at the top of the water storage tank ($T_{t,(n=Nn)}(i)$), with the temperature of the water exiting the PVT collector ($T_{cout}(i)$); see Components 4–5 in Fig. 2.

In order to avoid the requirement for the circulator pump (Component 3 in Fig. 2) to be switched on and off frequently, it is activated only when solar irradiance is greater than zero, in order to cool the PV module. However, fluid from the PVT collector is only sent to the heat exchanger coil in the tank when the temperature difference between collector and tank, $T_{cout}(i) - T_{t,(n=Nn)}(i)$, increases above a minimum set-point value, ΔT_{ON}, at which point the tank bypass is deactivated by switching the valve position. Fluid is circulated to the tank (through the heat exchanger coil) until $T_{cout}(i) - T_{t,(n=Nn)}(i)$ drops below a minimum set-point value ΔT_{OFF}, at which instant the bypass is activated again. In most domestic installations, ΔT_{ON}, ranges between 3 K and 10 K and ΔT_{OFF} is between 0.5 K and 1.5 K [64–66]. These values should be chosen carefully, as small changes in the settings might result in unexpected behaviour [67]. In this work, a symmetric band of allowed temperatures around the desired tank temperature is selected, ΔT_{ON} is set to 5 K, and hence $\Delta T_{OFF} = \Delta T_{ON}/2 = 2.5$ K [65]; thus in agreement with the guidelines mentioned above.

The pressure drop through the PVT fluid-loop is estimated in order to calculate the power consumed by the circulator pump (P_p), which will be taken from the electrical power output of the PVT collectors. The pressure drop, Δp, arises from losses in the closed hydraulic loop, and can be evaluated as the sum of major losses caused by friction and minor losses due to bends and fittings [19,25]. The pressure drop through the PVT collectors is estimated considering the friction losses in the collector tube and riser pipes (rectangular channels in the flat-box structure) and the minor losses due to the contraction and expansion from/to the collector tube to/from the riser pipes, using the expressions for sudden contraction and expansion provided in Ref. [68]. The flow within the PVT collector is laminar, such that $f = 64/Re$ for the S&T collectors [19,25], and $f = 96/Re_{Dh}$ for the flat-box structure [68]. Similarly, the pressure drop through the overall S-CHP system is evaluated by considering the total (volumetric) water flow-rate in the system and the estimated circuit length, tube diameters, number of elbows and fittings. The power consumed by the circulator pump is calculated by adding the pressure drop through the PVT collector and that through the rest of the fluid circuit, and multiplying this by the total (volumetric) flow-rate of water in the S-CHP system.

2.1.4. Electrical battery storage

The electrical output of the PVT collectors can be stored in batteries with an efficiency η_{bat}, through a standard switched charge controller of efficiency η_{cc} that connects both devices [69], as shown in Fig. 2. A DC to AC inverter, with an efficiency η_{inv}, is also considered [70,71]. The lead-acid battery integrated in this study has a monthly self-discharge rate (BSD) of 5%. This value is converted to an equivalent half-hourly self-discharge rate, BSD_{hh}, to be integrated in the S-CHP model.

The S-CHP system's electrical output is consumed directly by the household when there is a demand, by converting it to AC using an inverter. Any electricity excess is stored in the battery as defined by the actual charge current, I_C, and any electricity shortfall is supplied by the battery as defined by the actual discharge current, I_D. Here, I_C and I_D depend on the battery's specifications, specifically, the former on the maximum state of charge, SOC_{max}, and its maximum allowed charge current, I_{Cmax}, and the latter on the minimum state of charge, SOC_{min}, and its maximum allowed discharge current, I_{Dmax}.

When the battery is full or unable to store additional electricity due to technical limitations, that is, when the available charge current I_{C0} is larger than I_{Cmax}, the surplus energy is provided to the grid (E_{exp}). On the other hand, when the battery is empty or unable to meet the household electricity demand, the grid is assumed to be available to cover this demand (E_{grid}). Therefore, two possible situations arise: (i) an energy surplus, in which the S-CHP system generates more energy than the household demand ($E_{net} > 0$), and (ii) a shortfall, in which the system generates less energy than the demand ($E_{net} < 0$):

$$E_{net}(i) = E_{PVT}(i)\cdot\eta_{inv}\cdot\eta_{cc}-E_P-E_D(i), \quad (11)$$

where $E_{net}(i) = P_{net}(i)\cdot\Delta t$, $\Delta t = 0.5$ h is the time step, E_{PVT} is the electricity generated by the collectors, E_P is the electricity consumed by the pump, and E_D is the household electricity demand at time-step i.

A number of 12 V lead-acid batteries units are considered, with a maximum allowable charge and discharge current of $I_{Cmax} = I_{Dmax} = C/10$, where C is the battery capacity (100 Ah per single unit). The total number of batteries required varies with the number of PVT collectors (N), according to the expression: $C_T = 600\cdot N$. This correlation was selected following a preliminary analysis to ensure that the battery SOC is maintained within a reasonable range, and was a compromise between the energy storage capacity and the installed cost of the system, with the objective of minimising the number of batteries while also minimising the interaction of the investigated household(s)

with the grid.

The equations governing the interactions between the various electrical components are summarised in Table 1 and those modelling the battery performance features are summarised in Table 2.

2.2. Weather data and single-family reference house

The performance of the S-CHP systems in the domestic applications of interest were simulated by modelling a reference house in EnergyPlus [37], which provides estimates of the household's energy demands over a year, including the electricity needed for lighting, cooling and other household appliances, and the thermal energy required for space heating (SH) and domestic hot water (DHW). The reference house considered here is a double-glazed, 2-floor semi-detached household with a total floor area of ~115 m^2, and U-values of 0.26 W/(m^2·K) and 0.18 W/(m^2·K) for the façade and roof respectively. Typical occupancy profiles of 4 inhabitants (2 adults and 2 children) are considered, following the guidelines provided in the Spanish Building Code (*Código Técnico de la Edificación*) [56], which differentiates between working and non-working days, and provides loads and schedules for lighting and home appliances, as well as for occupancy and the air change rate. Based on the aforementioned building code [56], the following temperature set-points are set in the EnergyPlus household model to estimate the heating and cooling demands: (i) 20 °C primary and 17 °C secondary for SH (January to May and October to December), and (ii) 25 °C primary and 27 °C secondary for air conditioning (June to September).

The weather data (solar irradiance and ambient temperature) provided by EnergyPlus [72] are also used as inputs to the S-CHP model through the use of lookup tables. The direct normal and diffuse horizontal solar irradiance components are converted to a total incident solar irradiance, I_T, received on the tilted plane of the collector [73]. The collector tilt angle, β, is optimised for maximum annual solar irradiation at each location with the Photovoltaic Geographical Information System (PVGIS) online tool [74], resulting in the following values: $\beta = 32^\circ$ in Athens, $\beta = 38^\circ$ in London, and $\beta = 37^\circ$ in Zaragoza.

Energy demand profiles are also generated in EnergyPlus at half-hourly time-steps for the reference houses at the selected locations. The total electrical and thermal demands integrated over the annual period are: 18.3 kWh/m^2 and 30.7 kWh/m^2 in Athens, 24.3 kWh/m^2 and 54.7 kWh/m^2 in London, and 27.7 kWh/m^2 and 29.7 kWh/m^2 in Zaragoza, based on the monthly demand profiles shown in Fig. 5.

The cooling demand is found to vary strongly with location, and more than the other household energy demands, with the highest associated consumption experienced by the household located in Athens, where a greater amount of electricity is required to attain the desired comfort temperatures in the summer period (see dotted lines in Fig. 5) due to the higher irradiance level and higher ambient temperature at this location. A constant Seasonal Energy Efficiency Ratio (SEER) of 3 for the air-conditioning system is assumed at all locations for the calculation of the electricity consumption needed to satisfy the cooling demand. Furthermore, although the same lighting schedules and usage profiles for home appliances are considered in all three locations, the electrical consumption due to lighting varies slightly between the locations depending on the different available natural light levels.

Finally, the same DHW demand is experienced at all locations (see long dashed lines in Fig. 5), as expected given that: (i) the same DHW schedules and usage profiles are assumed, and (ii) variations in the DHW due to geographical variations in the mains water supply temperature are not considered, and thus the same mains water supply temperature is assumed for all locations. Finally, the highest SH demand occurs in London (see continuous lines in Fig. 5), which is attributed to the low irradiance levels (particularly in winter) together with the lower ambient temperature at this location. Conversely, the household located in Athens has the lowest SH demand.

Table 2
Battery performance features.

Description	Equation	Eq.
Battery capacity	$C = \frac{C_0}{V_B}$	(18)
Battery discharge capacity	$C_D(i) = (I_D(i)\cdot\Delta t)\cdot\eta_{bat}$	(19)
Battery charge capacity	$C_C(i) = (I_C(i)\cdot\Delta t)\cdot\eta_{bat}$	(20)
Change in battery capacity	$\Delta C(i) = C_C(i) - C_D(i)$	(21)
Battery capacity at next time-step	$C(i+1) = (C(i) + \Delta C(i))\cdot(1 - BSD_{hh})$	(22)
Battery state of charge	$SOC(i) = \frac{C(i)}{C}$	(23)

2.3. Economic assessment

Three economic parameters are used in the optimisation of the S-CHP systems of interest:

- Levelised Production Cost (*LPC*) of total (electrical and thermal) energy generated (LPC_{gen});
- Levelised Production Cost (*LPC*) of total household energy demand covered (LPC_{cov});
- Payback Time (*PBT*).

To this end, the capital/investment cost including all system components except the auxiliary heater and the O&M costs of the system ($C_{O\&M}$) are considered, as well as the utility (electricity and natural gas) savings (referred to as fuel savings, $FS_{S\text{-}CHP}$) and the costs incurred to satisfy the electrical and thermal demand of the household that cannot be covered (referred to as annual running costs, $C_{S\text{-}CHP}$). To estimate the annual fuel savings, $FS_{S\text{-}CHP}$, the total utility (electricity and natural gas) costs saved in the household due to the electricity and thermal (SH and DHW) energy demand covered by the S-CHP system are estimated (Eq. (24)). Then, these values, are converted into present worth values and added to obtain the Life Cycle Savings (FS_{LCS}), considering the market discount rate (d) and the fuel inflation rate (i_F), as follows:

$$FS_{S-CHP} = E_{cov}\cdot c_e + \frac{Q_{cov}}{\eta_{boiler}}\cdot c_{ng}, \quad (24)$$

Table 1
S-CHP system battery storage and grid interaction model equations.

Description	Energy surplus ($E_{net} > 0$)	Energy shortfall ($E_{net} < 0$)	Eq.
Available charge/discharge current	$I_{C0}(i) = \frac{P_{net}(i)}{\eta_{inv}\cdot\eta_{cc}\cdot V_B}$	$I_{D0}(i) = \frac{-P_{net}(i)}{\eta_{inv}\cdot V_B}$	(12)
Actual charge/discharge current	$I_C(i) = 0$	$I_D(i) = 0$	(13)
	$I_C(i) = I_{C0}(i)$	$I_D(i) = I_{D0}(i)$	(14)
	$I_C(i) = I_{Cmax}(i)$	$I_D(i) = I_{Dmax}(i)$	(15)
Battery charge/discharge power	$P_{BC}(i) = I_C(i)\cdot V_B$	$P_{BD}(i) = I_D(i)\cdot V_B$	(16)
Power exported/imported to/from grid	$P_{exp}(i) = P_{net}(i) - P_{BC}(i)$	$P_{grid}(i) = -P_{net}(i) - \eta_{inv}\cdot P_{BD}(i)$	(17)

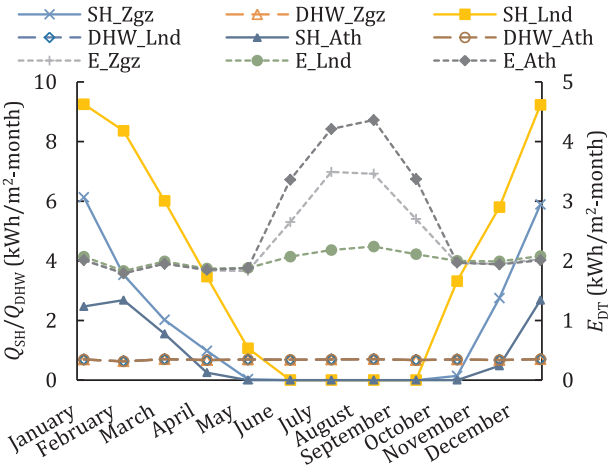

Fig. 5. Monthly space heating (SH), and domestic hot water (DHW) demands (left axis), and electricity demand (right axis) in kWh/m^2-month for the reference house located in each of three studied sites.

$$FS_{LCS} = \sum_{n=1}^{N} \frac{FS_{S-CHP}\cdot(1+i_F)^{n-1}}{(1+d)^n}, \tag{25}$$

where c_e and c_{ng} are the electricity and natural gas prices (€/kWh).

The fuel inflation rate (i_F) refers to the inflation rate considered for the annual fuel savings, FS_{S-CHP}, which comprises both electricity and natural gas savings.

Similarly, the net present value (*NPV*) of the S-CHP system can be estimated as follows:

$$NPV = C_0 + FS_{S-CHP}\cdot\frac{1}{d-i_F}\cdot\left[1-\left(\frac{1+i_F}{1+d}\right)^n\right], \tag{26}$$

where C_0 is the total investment cost of system, n is the system's lifetime (assumed to be 25 years) [75,76]. The *PBT* can be then calculated as the time (n) when $NPV = 0$.

On the other hand, the *LPC* is calculated as the total cost incurred per kWh over the system's lifetime:

$$LPC = \frac{L_e}{E_{Teeq}}. \tag{27}$$

where E_{Teeq} is the total "equivalent" electrical energy (in kWh$_{eeq}$) that allows results to be compared to other renewable energy technologies. This term is calculated by converting the total primary energy (E_{Tpe}) to equivalent electrical energy using the electricity conversion factors specific for each country where the analysis is undertaken (see Table 4). To estimate the LPC of energy generated (LPC_{gen}), the total electricity (E_{PVT}) and thermal energy (Q_{cov}) generated are converted to primary energy through the corresponding conversion factors for electricity and gas. Meanwhile, to estimate the LPC of energy demand covered in the household (LPC_{cov}), only the electricity (E_{cov}) and thermal (DHW and SH) energy (Q_{cov}) covered are considered. The annual CO_2 emissions displaced are also estimated considering electrical and thermal energy covered and the conversion factors from electricity and natural gas specific for each country (see Table 4).

The levelised cost (L_e) in Eq. (27) is the annualised life cycle cost (capital + running costs) associated with the system. The life cycle cost (*LCC*) is calculated by substituting FS_{S-CHP} by C_{S-CHP} in Eq. (26), where C_{S-CHP} is given by:

$$L_e = \frac{LCC}{\frac{1}{d-i_F}\left[1-\left(\frac{1+i_F}{1+d}\right)^n\right]}, \tag{28}$$

$$C_{S-CHP} = E_{grid}\cdot c_e + \frac{Q_{aux}}{\eta_{boiler}}\cdot c_{ng} + C_{O\&M}, \tag{29}$$

Table 3
Price breakdown of S-CHP components [88].

Component	Value	Unit	Reference
Benchmark (S&T) PVT collector	380	€/collector	[78]
PC 3 × 2 flat-box PVT collector	301	€/collector	[26]
Pump station	265	€	[79,80]
Controller	110	€	[81]
Expansion vessel	140	€	[82]
Water storage tank	$0.874\cdot V_t$ (L) + 763.5	€	[83]
Pipes (including insulation)	11	€/m	[82]
Heat transfer fluid	3.3	€/L	[84]
Mounting	59	€/collector	[79,80]
Lead-acid batteries	$69/840\cdot C_T$	€	[85]
System installation	1800	€	[77]

where E_{grid} is the electricity imported from the grid and Q_{aux} the auxiliary heat required to satisfy the rest of the household's electrical and thermal demands, respectively, that are not covered by the system.

The S-CHP system's investment cost is estimated from price lists available from solar retailers in the EU (VAT included). The main costs of system are associated with the storage tank, the PVT collectors, the pump station, the electronic controller and the piping and fixings. The cost of the storage tank is estimated using a correlation based on market prices of existing tanks across a range of storage volumes. The total installation costs are also considered [77]. The auxiliary heater price is not considered as it is assumed that the households already have one installed. Table 3 details the price breakdown.

Actual electricity and natural gas prices for domestic consumers in the three locations: Athens (Greece), London (UK) and Zaragoza (Spain) are used to calculate the running costs, the values considered are excluding taxes and levies. Band DC[1] (2500 kW h < consumption < 5000 kW h) is selected for the electricity prices, as the total household electricity consumption is between ~2800 kW h and ~3500 kW h [86]. For the natural gas prices, Band D1 (consumption < 20 GJ, 5555 kWh) is selected for Athens and Zaragoza where the total natural gas consumption to satisfy the combined household demands for SH and DHW, assuming a boiler efficiency of 90.1% [87], amount to ~3800 kWh and ~2400 kWh respectively at the two locations, whereas Band D2 (20 GJ, 5555 kWh < consumption < 200 GJ, 55555 kWh) is selected for London where the total natural gas consumption is ~7000 kWh [86]. Table 4 details the specific values selected. It should be noted that the natural gas price for London is significantly lower than in the other cases due to the higher band required to satisfy the demand. If the demand was lower than 5555 kWh, the natural gas price would increase to 0.0768 €/kWh [88].

The current feed-in-tariffs (FITs) available in the UK (0.048 €/kWh) and Athens (0.105 €/kWh) [89,90] are not included in the technoeconomic optimisation as in Spain there is currently no such incentive and also because the aim here is to compare the economics of these systems without financial incentives in place. However, FITs are considered at the end of the analysis in order to examine the role of this incentive in improving their economic proposition. Conversion factors to CO_2 emissions specific to each location are used to obtain the annual displaced emissions [91–93] (see Table 4). A market discount rate of 3.5% is considered, applicable to projects with up to 30-year lifetimes [94], and the fuel inflation rate is set to 2.7% based on the inflation rates in the different countries under study [95,96], which is in line with the fuel inflation rate considered in previous studies [97].

Considering the electricity and natural gas prices and the conversion factors to primary energy detailed above, together with the household energy demand in each country, Table 5 summarises the annual

[1] The electricity and natural gas prices vary depending on the annual energy consumption within different bands: D1, D2 and D3 for natural gas consumption, and DA, DB, DC, DD and DE for electricity consumption.

Table 4
Economic and environmental parameters in the different countries.

	Prices (€/kWh$_{fe}$)			Conversion factor (kWh$_{pe}$/kWh$_{fe}$)		CO_2 emission factor (kgCO_2/kWh$_{fe}$)	
	Electricity*	Natural Gas*	FIT	Electricity	Natural Gas	Electricity	Natural Gas
Spain	0.1796	0.0879	0	2.37	1.20	0.357	0.252
UK	0.1479	0.0466	0.0476	3.07	1.22	0.410	0.184
Greece	0.1185	0.0844	0.1050	2.90	1.05	0.989	0.196

fe = final energy; pe = primary energy; FIT = Feed-In-Tariff.
* Prices excluding taxes and levies.

Table 5
Annual results of the household energy consumption and associated running costs incurred by conventional means.

	Athens, Greece	London, UK	Zaragoza, Spain
E_{TDeq} (kWh$_{eeq}$/year)	4291	5296	4902
C_{conv} (€/year)	540	739	831
LPC_{conv} (€/kWh$_{eeq}$)	0.143	0.140	0.184

electricity and thermal energy (both SH and DHW) household demand converted to equivalent electricity as detailed above (E_{TDeq}), the annual household running costs (C_{conv}) (equivalent to buying natural gas and electricity from the grid to satisfy all household demand by conventional means), and the equivalent levelised production cost (LPC_{conv}) of the household (estimated as C_{conv}/E_{TDeq}).

In Table 5, we can observe the importance of the utility prices that significantly affect the economics of the S-CHP system. In particular, despite the significantly lower annual energy demands compared to London, the higher electricity and natural gas prices in Zaragoza (20% and 47% higher, respectively) mean that the *LPC* of the system in London is lower because the household inhabitants spend less money to satisfy their energy demands by conventional means. Due to the lower electricity price in Athens with respect to Zaragoza (~34% lower), the *LPC* in this case is even lower. Consequently, and as will be demonstrated in the next section, it is more challenging to achieve a cost-effective renewable system capable of competing with conventional non-renewables in London and Athens than in Zaragoza.

2.4. System sizing and technoeconomic performance assessment

The objective of this work is to compare, from a technoeconomic perspective, optimised S-CHP systems based on two PVT collector designs: (i) a novel polycarbonate flat-box design, which was selected as the most promising such design in previous research [26], and (ii) a benchmark reference (sheet-and-tube) design. Three different climates are selected for this study, representing: (i) Mediterranean (Athens, Greece), (ii) temperate oceanic (London, UK), and (iii) semi-arid (Zaragoza, Spain). A methodology is developed to obtain in a systematic way optimally sized and operated S-CHP system configurations at the three locations. The methodology is presented below.

Firstly, the identification of the most appropriate design variables that will be used later to optimise the system requires an assessment of the various performance parameters of the S-CHP system. This exercise is performed in the semi-arid climate of Zaragoza (Spain), which was selected as an intermediate between the two other case studies, with solar irradiance conditions and household energy demands that also lie in between the two other locations (Athens and London). Then, for each of the aforementioned locations, the optimal number of PVT collectors, N, and the storage tank size, V_t, are determined for an average week in each month of the year, selected in this work to be the week over which the mean and standard deviation of the solar irradiance are closest to the mean and standard deviation over the whole month. The analysis is undertaken in half-hourly steps, using an in-house algorithm developed in MATLAB. The results obtained for the optimal values of N and V_t are then averaged for the 12 months to obtain annual averages.

After the S-CHP system has been sized in this manner, the PVT collector flow-rate, V_P, (determined to be the most important operational parameter) is optimised for each month of the year. As before, the optimisation is undertaken in half-hourly steps over an average week in each month. The weekly results are then multiplied by a weighting factor based on the number of days per month, and summed to obtain an estimate of the annual energy, cost and emission savings. Based on these results, the *PBT* and *LPC* of the optimal system configuration are estimated for S-CHP systems featuring both polymeric flat-box and benchmark sheet-and-tube PVT collector designs, and the results are compared at the three locations. Finally, performance profiles on selected days for both collector designs are presented and discussed.

3. Results and discussion

3.1. Selection of key performance indicators for system sizing

The aim of this first exercise is to identify the decision factors based upon which the S-CHP system can be optimised, given irradiance, ambient temperature, and household energy-demand data. The system performance indicators are evaluated for the case of Zaragoza, which was selected amongst the locations of interest here as it is an intermediate case between those of Athens and London. As mentioned above, the analysis is undertaken in half-hourly steps over an average week in each month. The monthly outputs are then weighted to obtain annually averaged results.

Two parameters are varied in sizing the S-CHP system: the number of PVT collectors (N) and the ratio V_t/N. The PVT collector flow-rate (V_p) is kept constant at 50 L/h (per collector), which is within the flow-rate range recommended by the PVT manufacturer [53]. The performance indicators considered in this research are:

- Levelised production cost per unit equivalent electrical energy generated (LPC_{gen}) (€/kWh$_{eeq,gen}$).
- Levelised production cost per unit equivalent electrical energy covered (LPC_{cov}) (€/kWh$_{eeq,cov}$).
- System payback time (*PBT*).
- Grid interaction: difference between the electricity imported (E_{grid}) and exported (E_{exp}) from/to the grid to satisfy the household electricity demand.
- Thermal energy balance: difference between the auxiliary heating required to cover the household thermal energy demand (Q_{aux}) and the rejected excess heat (Q_{dump}) to avoid tank overheating.
- Percentage of thermal (SH and DHW) and electrical demand covered in the household.

Initially, a preliminary analysis was undertaken to select a reasonable value for the ratio V_t/N. A flow rate value of 90 L/collector was found to provide a high level of thermal energy demand, so this is the value considered as a starting point of the sizing exercise. Then, for the system sizing in each location, first of all, the number of PVT collectors (N) is varied up to 33, which corresponds to a total PVT array area of around 50 m^2 and the maximum useable roof area on the single family

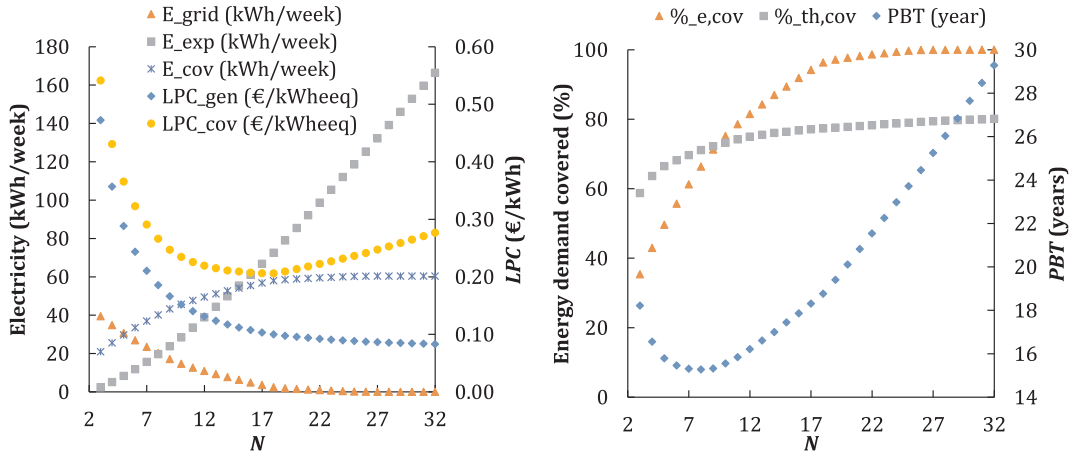

Fig. 6. Annually averaged (left) weekly electricity imported (E_{grid}), exported (E_{exp}) and covered (E_{cov}), and *LPC* per unit of equivalent electricity generated (LPC_{gen}) and covered (LPC_{cov}), and (right) *PBT* and percentage of household electrical ($\%_{e,cov}$) and thermal energy ($\%_{th,cov}$) demands covered by a S-CHP system installed in Zaragoza (Spain), with different number of PVT collectors (N) and V_t/N fixed at 90 L/collector.

dwelling-type chosen for this study. The tank volume V_t also varies accordingly with N given the fixed ratio V_t/N.

Annually averaged results for Zaragoza are presented in Fig. 6. As expected, the number of PVT collectors (N) significantly influence the electricity generation, so the minimisation of the levelised cost of energy generated (LPC_{gen}, blue[2] diamonds, Fig. 6 left) leads to the maximum N, but in turn as the number of collectors increases, the electricity exported (E_{exp}, grey squares, Fig. 6 left) also increases. Similarly, the percentage of energy demand covered increases with N, reaching > 98% from 20 PVT collectors (shown by the orange triangles, Fig. 6 right), as well as the thermal demand covered, reaching an asymptote of 75–80% from 12 PVT collectors (grey squares, Fig. 6 right). Conversely, there is an optimum, within the studied range, of the levelised cost of energy covered (LPC_{cov}, yellow dots, Fig. 6 left) as well as an optimal system *PBT* (blue diamonds, Fig. 6 right). The reason is that these parameters consider the household energy covered (instead of all energy generated), as well as the S-CHP system investment cost (C_0). As a consequence, beyond a certain number of PVT collectors, the energy covered (E_{cov}) and associated cost savings reach an asymptote, while the system investment cost continues increasing with the number of PVT collectors. Furthermore, it is observed that the minimum grid interaction, that is, when $\Sigma E_{grid} = \Sigma E_{exp}$ (see Fig. 6 left) occurs for the same number of collectors as for the minimum *PBT*.

On the thermal generation side (results not shown in Fig. 6), as the number of collectors increases, the excess heat rejected to the ambient (Q_{dump}) increases significantly and almost linearly, while the auxiliary heat required to cover the household thermal energy demand (Q_{aux}) decreases at a far lower rate, plateauing at a minimum value that corresponds to the maximum fraction of thermal demand covered.

Based on these results, the number of PVT collectors (N) is fixed to 8 to minimise the *PBT* (see Fig. 6 right), and V_t/N is varied in the range 30–465 L/collector, which implies a storage tank volume between 250 and 3500 L. Larger tanks are not considered due to space constraints in a single-family house.

Fig. 7 shows the effect of varying the ratio V_t/N, for a fixed value of N, on important indicators that characterise the technoeconomic performance of the system. The results show that V_t/N does not notably influence the electricity generation, with the percentage of electricity demand covered slightly increasing with V_t/N (orange triangles in Fig. 7 right), due to the lower temperature of the water entering the PVT collector and hence the lower PV module temperature. Conversely, the percentage of thermal energy demand covered (grey squares in Fig. 7 right) shows a maximum value at around 80–130 L/collector, which coincides with the maximum thermal energy demand covered (Q_{cov}, yellow dots in Fig. 7 right), and hence with the minimum auxiliary heat needed (Q_{aux}, light blue crosses in Fig. 7 right). The reason for this is that at very low V_t/N the thermal energy stored in the tank is small, which limits the amount of thermal demand that can be covered. As the tank volume increases with V_t/N, more energy can be stored in the tank, increasing the demand covered, but at high V_t/N, due to the large thermal mass in the tank, the temperatures throughout the tank are lower, so the amount thermal energy (at the required temperature) that can be covered decreases.

The utilisation of energy stored in the tank is affected significantly by the demand profile, which is illustrated by the plot of the heat that is rejected to the ambient (Q_{dump}, dark blue diamonds in Fig. 7 right) due to overheating of the tank. For the smallest storage volume range (30–45 L/collector), the water at the top of the tank quickly reaches the minimum supply temperature of 35 °C early in the morning when there is also a peak in thermal energy demand. As the tank volume is increased to 60–80 L/collector, the rate of increase of tank temperature during the morning is slower, and less useful heat is provided during the early peak-demand period. Furthermore, the tank then reaches its maximum temperature limit later in the day during the low-demand period leading to a larger total amount of rejected heat. As the storage volume is increased further, the tank is able to store a larger amount of heat before reaching the maximum temperature limit and as a result Q_{dump} decreases again.

Similarly, turning now to selected economic indicators, the levelised cost of energy covered (LPC_{cov}, yellow dots in Fig. 7 left), levelised cost of energy generated (LPC_{gen}, blue diamonds in Fig. 7 left) and the system payback time (red crosses in Fig. 7 left) reach a minimum around the same V_t/N. Furthermore, it is observed that the thermal energy balance, $\Sigma Q_{aux} = \Sigma Q_{dump}$, occurs at $V_t/N \sim 120$ L/collector, which is similar to that corresponding to the optimal values of the aforementioned key performance indicators.

Based on these results, a set of decision factors were selected for use in the subsequent analyses. These factors are: (i) the minimisation of the *PBT*, which also leads to the minimum grid interaction on an annually averaged basis, and (ii) the minimisation of the LPC_{cov}, which also leads to the maximum thermal energy demand covered and hence the minimum auxiliary heat required.

3.2. Technoeconomic optimisation for system sizing

Following the procedure described in Section 3.1, the S-CHP system

[2] For interpretation of colour in Figs. 6–9, the reader is referred to the web version of this article.

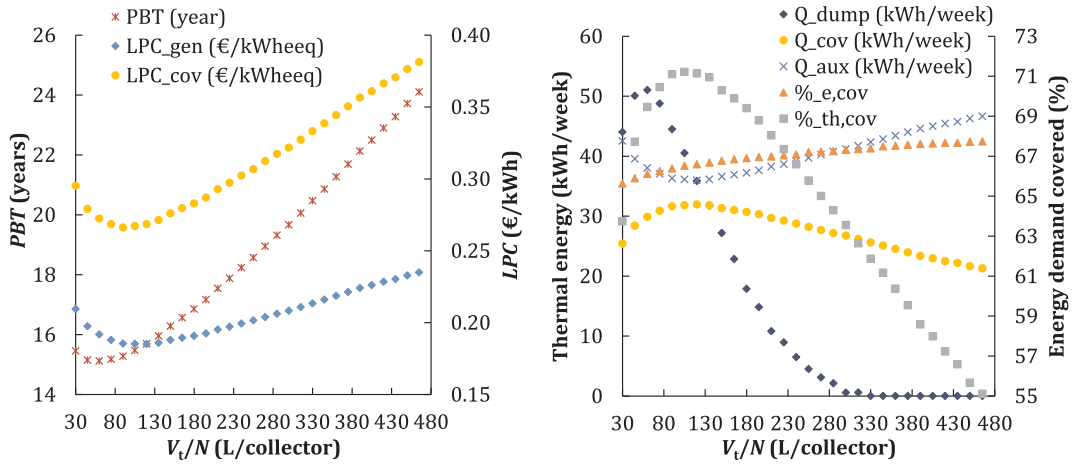

Fig. 7. Annually averaged (left) *PBT* and *LPC* per unit of equivalent electricity generated (LPC_{gen}) and covered (LPC_{cov}), and (right) weekly thermal energy demand covered (Q_{cov}), rejected excess heat (Q_{dump}), auxiliary heating (Q_{aux}), percentage of household electrical ($\%_{e,cov}$) and thermal energy ($\%_{th,cov}$) demands covered by a S-CHP system installed in Zaragoza (Spain), with different V_t/N ratios.

sizing (number of collectors, N, and water storage tank volume, V_t) is optimised for reference households located in the three locations of interest to this work (Athens, London and Zaragoza). As in the previous section, only the case of Zaragoza is considered here in detail, since it presents an intermediate case as explained before, and equivalent results are obtained in the other cases. Key results relating to the performance of optimised systems installed at the other two locations over the course of the year are also shown in order to compare the systems' performance at the different locations.

Firstly, the number of PVT collectors (N) is varied up to 33, with V_t/N fixed at 90 L/collector, such that the tank volume (V_t) varies according to N. These results, shown already in Fig. 6, indicate that to minimise the LPC_{cov}, the number of PVT collectors required is significantly higher (some months more than double) than to minimise the *PBT*; specifically, between 9 and 23 PVT collectors in the former case and 4–16 in the latter for the household located in Zaragoza. This leads to a greater interaction with the electricity grid, exporting a significant amount of electricity generated from the PVT system (and an averaged grid interaction, $\Sigma E_{grid} - \Sigma E_{exp}$, of 70.1 kWh/week in the former case *vs.* 0.6 kWh/week in the latter). Due to the larger S-CHP dimensions (N and V_t) in the former case, the *PBT* is also considerably higher (20 *vs.* 8 years based on the annually-averaged results), as the increase in fuel savings do not outweigh the higher investment cost. As stated above, the number of collectors (N) is selected to minimise the *PBT*, hence 8 PVT collectors are selected, with which grid interaction ($\Sigma E_{grid} - \Sigma E_{exp}$) is also minimised. In Fig. 6 it is also observed that from 8 PVT collectors the slope of the LPC_{cov} significantly declines, decreasing at much lower extent from there onwards until it reaches a minimum. Furthermore, between 7 and 8 PVT collectors, the excess of heat rejected to the ambient (Q_{dump}) is very close to the auxiliary heat (Q_{aux}), so the excess of thermal energy and auxiliary heat needed is balanced.

With the number of PVT collectors selected ($N = 8$, for a fixed $V_t/N = 90$ L/collector), the S-CHP system performance is assessed in each month in order to obtain the weekly equivalent electricity covered (E_{Teeq}), the associated fuel savings ($FS_{S\text{-}CHP}$) and the weekly running costs ($A_{S\text{-}CHP}$). Following this assessment, the monthly results are added to obtain the annual fuel savings (537 €/year), which in this case lead to a *PBT* of 14.7 years ($C_0 = 7252$ €), and the equivalent electricity covered (3016 kWh_{eeq}/year), and annual running costs (374 €/year), which lead to an LPC_{cov} of 0.257 €/kWh_{eeq}.

To verify whether the value of V_t/N used initially was optimal, and following the procedure detailed in Section 3.1, this parameter is varied in the range 30–465 L/collector. The results show that, averaged over an annual period, V_t/N = 90–105 L/collector leads to the lowest LPC_{cov} (see yellow dots in Fig. 7 left) which coincides approximately with the V_t/N that maximises the covered thermal-energy demand (grey squares in Fig. 7 right). The minimum *PBT* is achieved at a lower V_t/N, however the variation in *PBT* is relatively small (15.1–15.5 years, dark red crosses in Fig. 7 left) over the corresponding range of V_t/N values between 60 and 105 L/collector. Conversely, the excess heat rejected to the ambient (Q_{dump}, dark blue diamonds in Fig. 7 right) decreases notably (by around 21%) as V_t/N is increased from 60 to 105 L/collector. Based on these results, a V_t/N of 90–100 L/collector is considered a good compromise and, as results for $V_t/N = 90$ L/collector are already estimated from previous analysis, $V_t/N = 100$ L/collector is selected in this case for further analysis. The results show that the slight increase in the annual fuel savings in this case, does not outweigh the higher investment cost (C_0) due to the larger tank ($V_t = 0.80\ m^3$ *vs.* $0.72\ m^3$ in the former case).

Based on the aforementioned analyses, the system size selected for the household in Zaragoza comprises 8 PVT collectors and a storage tank with $V_t = 0.72\ m^3$. This leads to $V_t/A_{cT} = 58.4\ L/m^2$ (PVT collector area, $A_c = 1.54\ m^2$), which is inside the range established by the Spanish Building Technical Code ($50 < V_t/A_{cT} < 180$, in L/m^2) [56].

Finally, the effect of Feed-In-Tariffs (FITs) on the economics of the systems was also considered. At present, there is no FIT available to PV installations in Spain. Therefore, in order to understand the role of this incentive in Spain and specifically for the system in Zaragoza, we considered the FIT presently available to small PV installations in the UK (0.0476 €/kWh) [89]. The results show that in this case the *PBT* is reduced by 1.5 years due to the FIT, achieving a PBT_{FIT} of 13.5 years.

A similar procedure to that described for the location of Zaragoza is conducted for Athens and London leading to the sizing of these systems. The weekly (electrical and thermal) energy results during the different months of the year for the systems sized for the households located in Athens and London are shown in Fig. 8. The results for the location of Zaragoza are not shown as they are between the former locations, so the equivalent conclusions can be drawn. As expected, the larger auxiliary heat needs (Q_{aux}) occur in the winter months (see green squares in Fig. 8), particularly from December to February, which is attributed to the higher SH demand and also lower irradiance during those months (see Fig. 8). Comparing the results of the different locations, it is observed that, as expected, the auxiliary heating needs (Q_{aux}) in London in winter are higher than in Athens (and Zaragoza although not shown here), due to the higher SH demand in the former (see Fig. 5).

In Athens, the more electricity is imported from the grid (E_{grid}) in the summer months, from June to September (see orange diamonds in Fig. 8 left), due to the higher cooling demand (see Fig. 5), which also leads to less electricity exported to the grid (E_{exp}) over this period. The solar irradiance is also higher in summer months, and is available

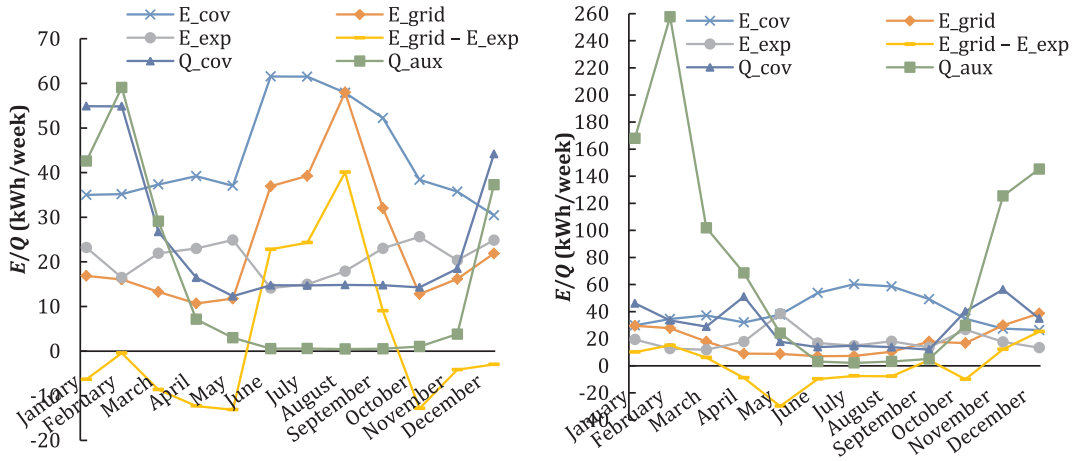

Fig. 8. Weekly energy results (kWh/week) in each month of the S-CHP system installed in (left) Athens (Greece) with $N = 9$, $V_t/N = 90$ L/collector, and (right) London (UK) with $N = 11$, $V_t/N = 90$ L/collector.

during the hours in which cooling demand is highest, leading to a higher total electricity demand covered (E_{cov}) in summer months. Due to the higher cooling demand, the grid balance ($\Sigma E_{grid} - \Sigma E_{exp}$) is positive in some summer months in Athens (Fig. 8 left), while in the case of London it is negative in summer months, which implies that electricity is exported to the grid (E_{exp}) in the latter case (Fig. 8 right).

3.3. PVT collector operation optimisation

With the optimal S-CHP system size determined at each location, the flow-rate per collector (V_p) is optimised in each month, within the range of 5–300 L/h. Lower collector flow-rates lead to higher ΔT across the PVT collector, whereas high flow-rates are typically preferred to maintain the PV module at low temperature to achieve the maximum electrical efficiency. However, high flow-rates lead to higher pumping work and thus less net electricity available. The results show that the same PVT collector flow-rate in each case study leads to the minimum LPC_{gen}, LPC_{cov} and *PBT*, as well as to the maximum thermal energy demand covered (Q_{cov}) and hence minimum auxiliary heat (Q_{aux}) needed and maximum percentage of thermal energy demand covered.

As with the previous section, only the case of Zaragoza is shown in detail here as similar results are obtained in the other cases. In all the cases, the results show that low PVT collector flow-rates are recommended to maximise the thermal energy demand covered for all the months and hence minimise the *PBT* (see annually averaged results for Zaragoza location in Fig. 9). However, low PVT collector flow-rates lead to higher excess of heat rejected to the ambient (Q_{dump}) (see dark blue diamonds in Fig. 9 right). As shown in Fig. 9 (right), a zero net thermal energy balance ($\Sigma Q_{aux} = \Sigma Q_{dump}$) is obtained in Zaragoza for $V_p \sim 65$ L/h. It is observed that the electrical demand covered only varies slightly over the range of PVT collector flow-rates, between 66.8% at low flow-rate to 65.6% at high flow-rate (see orange triangles in Fig. 9 right), which is attributed to the higher electricity consumption of the circulator pump reducing the electricity available to satisfy the household demand.

The results show that if the PVT collector flow-rate is fixed to 30 L/h throughout the year (optimal annually averaged as shown Fig. 9 left), slightly higher annual fuel savings are achieved, which leads to a 0.4% lower *PBT* and a 0.6% lower LPC_{cov} than with the previous constant flow-rate of 50 L/h. The effect of incorporating a variable-speed pump, which is adjusted on a monthly basis to provide the optimal flow-rate to the PVT collectors in each month, was also investigated. The *PBT* was found to be 0.3% lower and the LPC_{cov} was 0.1% lower than with the constant flow-rate of 30 L/h. Thus, in this case, it can be concluded that the higher cost of the variable speed pump (which has not been considered in this calculation) might not outweigh the slight improvement in the system performance.

Furthermore, if the goal is to minimise the thermal energy balance ($\Sigma Q_{aux} - \Sigma Q_{dump} \sim 0$), a constant PVT collector flow-rate of 65 L/h should be selected (see Fig. 9 right), with which a *PBT* of 14.9 years and

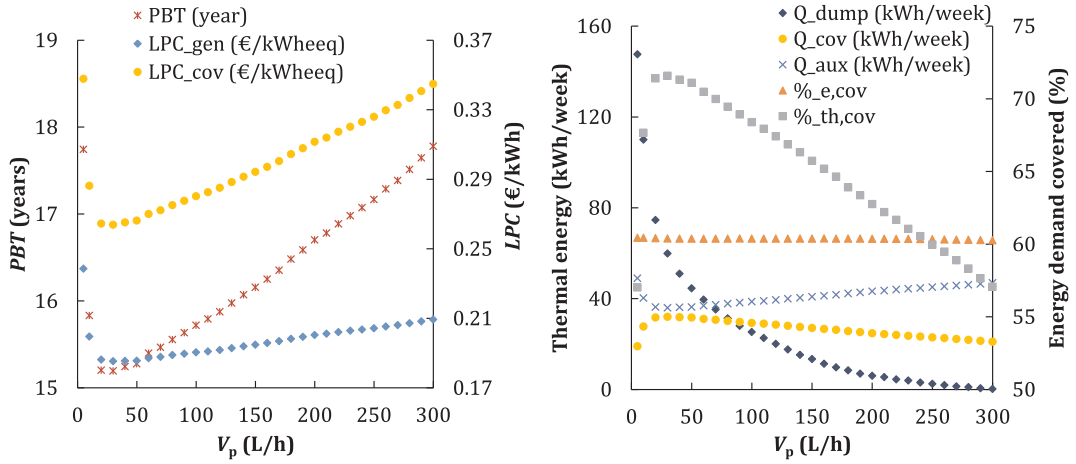

Fig. 9. Annually averaged (left) *PBT* and *LPC* per unit of equivalent electricity generated (LPC_{gen}) and covered (LPC_{cov}), and (right) weekly thermal energy demand covered (Q_{cov}), rejected excess heat (Q_{dump}), auxiliary heating (Q_{aux}), percentage of household electrical ($\%_{e,cov}$) and thermal energy ($\%_{th,cov}$) demands covered by a S-CHP system ($N = 8$ & $V_t = 0.72\ m^3$) installed in Zaragoza (Spain), with different collector flow-rates (V_p).

an LPC_{cov} of 0.261 €/kWh$_{eeq}$ are achieved. In this case, when the total electricity PVT generation is considered, an LPC_{gen} of 0.178 €/kWh$_{eeq}$ is estimated. If all of the household energy demand was instead satisfied by conventional means (buying natural gas and electricity from the grid), as detailed in Table 5, an equivalent LPC_{conv} of 0.184 €/kWh$_{eeq}$ is obtained. Therefore, it can be concluded that the proposed S-CHP system based on the polymeric flat-box PVT collector is a promising alternative to a business-as-usual scenario when installed in Zaragoza, even without the need of government incentives. If a FIT equivalent to the one available in the UK was in place (see Section 2.3), the *PBT* would decrease to ~13.5 years and the LPC_{gen} to 0.167 €/kWh$_{eeq}$. Both payback times are significantly lower than the S-CHP system lifetime (estimated as 25 years). Consequently, during the last ~10 years the system is expected to generate profits to the household, irrespective of whether FIT are available. An additional incentive of this system is the potential CO_2 emissions reduction, estimated as ~1.65 tons CO_2/year.

The same analysis as above is undertaken when the benchmark PVT collector (sheet-and-tube design) is integrated into the S-CHP system, and the results are compared to those from the polymeric flat-box PVT collector system. As before, the results of the optimal S-CHP system show that low PVT collector flow-rates are also recommended to maximise the thermal energy demand covered throughout the year and hence minimise the *PBT*. To reach the zero net thermal energy balance ($\Sigma Q_{aux} = \Sigma Q_{dump}$), a slightly higher collector flow-rate is also recommended (V_p ~ 50 L/h in this case). Slightly lower electrical demand covered is achieved with the benchmark PVT collector (65.5% compared to 66.7% for the PC flat-box collector) across the range of PVT collector flow-rates, due to the less effective heat extraction as shown in the PVT thermal efficiency curve in Section 2.1. With a constant PVT collector flow-rate of 50 L/h, a *PBT* of 16.3 years, an LPC_{cov} of 0.273 €/kWh$_{eeq}$ and an LPC_{gen} of 0.190 €/kWh$_{eeq}$ are achieved. The *PBT* of the benchmark PVT S-CHP system is higher than that of the equivalent polymeric flat-box PVT-based system by an additional 1.4 years, and this can be attributed mainly to the higher investment cost of the benchmark PVT collector (380 €/collector *vs.* 301 €/collector).

3.4. Comparison of optimised S-CHP systems at different locations

Table 6 summarises the features of the optimised S-CHP system configurations for both the polymeric flat-box PVT and the benchmark PVT systems in the three locations studied in the present work. It is observed that the optimal sizing and operating parameters of the system are within a relatively small range for the three locations (between 8 and 11 PVT collectors, a hot water storage tank volume of 0.68–0.83 m^3 and a PVT collector flow-rate between 30 and 65 L/h), despite the differences in terms of irradiance levels, ambient temperature, and household energy demand (see Section 2.2). As expected, a higher number of PVT collectors and a larger storage tank together with lower PVT collector flow-rates are required in London due to the lower irradiance levels together with the significantly higher SH demand (around twice the equivalent to Zaragoza and four times higher than the SH demand in Athens).

Table 6 also shows the annual energy generation results of the optimised S-CHP system configurations. The results show that, at all locations, the polymeric flat-box PVT-based S-CHP system outperforms the benchmark sheet-and-tube equivalent system due to the more efficient heat extraction of the former, which increases both the electricity and thermal energy generated by the system.

Of the three locations, Athens has the highest electricity generation (E_{PVT}), as well as the highest household electricity demand covered (E_{cov}), due to the slightly larger optimal collector array size than for Zaragoza and significantly higher irradiance levels than London. Nevertheless, it is found that more electricity should be imported from the grid (E_{grid}) for the Athens case which is attributed to the higher electricity demand, specifically in summer months, due to the higher cooling demand. The results of the thermal energy demand covered show that Athens achieves the highest percentage (61.3%), despite the lowest total amount of thermal energy covered by the S-CHP system (Q_{cov}). This is attributed to the low thermal energy demand (see Fig. 5), which also leads to the lowest auxiliary heat requirement (Q_{aux}). Conversely, in London it is only possible to cover ~29% of the total thermal energy demand, due to the high household thermal energy demand together with the low irradiance levels.

When the system economics are considered, in particular the utility costs, different conclusions can be drawn. As shown in Table 7, the lowest *PBT* is achieved when the S-CHP system is located in Zaragoza, around 7 years and almost 13 years lower than in Athens and London, respectively. The main reason is attributed to the significantly higher utility prices in Spain compared to the other locations (see Table 4), specifically, ~21% and ~89% higher electricity and natural gas prices respectively than in the UK and ~52% and ~4% higher electricity and natural gas prices respectively than in Greece. As a consequence, the fuel savings ($FS_{S\text{-}CHP}$) thanks to the integration of the proposed S-CHP systems in the household are considerably higher for Zaragoza, despite a lower electricity demand coverage than for Athens and a slightly lower thermal energy demand coverage than for London. Therefore, it can be concluded that the utility prices strongly affect the economics of renewable systems, when the energy and associated costs savings are considered. Similar conclusions can be drawn when considering the LPC, as this parameter considers the annual running costs incurred in the household to cover the thermal and electrical demand, and hence it is very sensitive to the utility prices.

In all previous analyses, the utility prices considered are excluding taxes and levies. When all taxes and levies are included, utility prices

Table 6
Annual energy results (kWh/year) and annual household electrical and thermal energy demand covered (%) of the optimised S-CHP system configurations in households located in each of the assessed locations.

	Athens, Greece		London, UK		Zaragoza, Spain	
	Polymeric flat-box PVT	Benchmark PVT	Polymeric flat-box PVT	Benchmark PVT	Polymeric flat-box PVT	Benchmark PVT
N	9		11		8	
A_{cT}	14.0 m^2		17.0 m^2		12.4 m^2	
V_t	0.68 m^3		0.83 m^3		0.72 m^3	
V_p	50 L/h	50 L/h	30 L/h	30 L/h	65 L/h	50 L/h
E_{PVT}	3674	3603	3025	2977	3487	3395
E_{cov}	2263	2262	1823	1822	2096	2091
E_{grid}	1249	1251	957	958	1058	1063
E_{exp}	1057	994	909	866	1044	968
Q_{cov}	1283	1264	1634	1589	1600	1599
Q_{aux}	811	839	3939	3984	1931	1929
$\%_{th,cov}$	61.3	60.1	29.3	28.5	45.3	45.3
$\%_{e,cov}$	64.4	64.4	65.6	65.5	66.5	66.3

Table 7
System economics of the optimised novel polymeric flat-box PVT-based and benchmark PVT-based S-CHP systems in the three locations, with and without financial incentives (utility prices excluding taxes and levies).

			PBT (years)	LPC_{cov} (€/kWh$_{eeq}$)	LPC_{gen} (€/kWh$_{eeq}$)
Athens (Greece)	Polymeric flat-box PVT	No FIT	22.0	0.232	0.155
		FIT†	16.8	0.232	0.128
	Benchmark PVT	No FIT	24.6	0.249	0.168
		FIT†	18.9	0.211	0.142
London (UK)	Polymeric flat-box PVT	No FIT	27.7	0.322	0.219
		FIT+	24.4	0.305	0.207
	Benchmark PVT	No FIT	31.2	0.345	0.237
		FIT+	27.5	0.329	0.226
Zaragoza (Spain)	Polymeric flat-box PVT	No FIT	14.9	0.261	0.178
		FIT*	13.5	0.244	0.167
	Benchmark PVT	No FIT	16.3	0.273	0.190
		FIT*	14.9	0.258	0.179

* FIT = 0.048 €/kWh.
\+ FIT = 0.048 €/kWh.
† FIT = 0.105 €/kWh.

increase considerably (see first two columns on Table 8), which leads to a more favourable *PBT* for the proposed solar solution. As shown in Table 8, in this case, all the *PBT* are below the system's lifetime (~25 years), even when FIT are not considered. Conversely, the LPC_{cov} and LPC_{gen} increase, as higher prices increase the total annual running costs of the household. It should be noted that, in this case (which is more realistic as it considers the taxes and levies that the end-user will have to pay), a reasonable *PBT* (15.6 years) is also obtained in Athens without the need of FIT. Thus, it can be concluded that the *PBT* values obtained in Zaragoza and Athens are on the order of magnitude expected for this type of solar system installed in the South of Europe. The results show that, in Northern climates, such as the UK, characterised by lower irradiance levels and high household space heating demand, it might be more beneficial to size these S-CHP systems for the provision of DHW-only, instead of DHW and SH, as this will lead to a smaller system size required to satisfy a more constant hot water demand throughout the year. However, this alternative has not been assessed here as it is beyond the main scope of this work. Nevertheless, in the aforementioned climates, to promote the installation of these S-CHP systems the implementation of some financial incentive might still be necessary to lower the *PBT* further.

Finally, the potential emission reductions that can be achieved by the integration of the optimised S-CHP systems into households are found to be sensitive to the country where these systems are installed. The high CO_2 emission factor of the electricity grid in Greece (see Table 4) makes these systems particularly promising in this location, where they have the potential to displace around 3.87 tons CO_2 over a year, compared to the 1.54 and 1.65 tons CO_2/year for London and Zaragoza, respectively. By comparison, PV-only solutions displace 3.56, 1.21, 1.22 tCO_2/year (or, up to 20–25% lower) from the same area, and 10.85, 3.41, 3.98 tCO_2/year for the same total cost which, however, would correspond to installed PV-covered surface areas of 43, 49 and 41 m^2, respectively. The benefits, therefore, appear noteworthy in the case of space restrictions.

3.5. Daily performance analysis of optimised configurations

3.5.1. Optimised S-CHP system in Zaragoza

Figs. 9 and 10 show the selected performance profiles of the optimised S-CHP system ($N = 8$ and $V_t = 0.72$ m^3) in Zaragoza, over three days in winter (February) and three days in summer (July), respectively. Results are compared in the plots for the PC 3 × 2 flat-box PVT system (for which V_p is set to the optimal 65 L/h) and the benchmark S &T PVT system (for which V_p is set to the optimal 50 L/h). In the first two figures, the differences in the performance and operation of both systems between cloudy and sunny days are presented. It should be noted that the elevated total irradiance (I_T) peaks (Fig. 10 left) in winter are due to the correction factors considered to calculate the solar irradiance at tilted angle.

The detailed results concerning the thermal performance indicate that on the selected winter days, for both the optimised polymeric flat-box PVT-based and benchmark S-CHP systems, around 52% of the entire thermal (DHW plus SH) demand is covered in Zaragoza. Both S-CHP systems perform very similarly because the improvement in the thermal performance of the polymeric flat-box PVT collector compared to the benchmark PVT collector (see Section 2.1) is too low to result in a noticeable difference on an annual basis (Fig. 10 left). However, as shown in previous sections, considerably better economics are achieved with the polymeric flat-box PVT-based S-CHP system, thanks to the lower PVT collector price. It is observed that the early thermal energy demand peak due to SH requirement (orange squares in Fig. 10 left) on the first of the three winter days cannot be covered by the S-CHP systems, because the temperature of the water in the storage tank at the beginning of the day is too low (a result of very low solar irradiance received on the previous day). However, on the second day, thanks to the larger amount of thermal energy stored in the tank, part of the early morning SH demand peak can be covered with the S-CHP system, as well as most of the thermal energy demand later in the day.

In Fig. 10 (right) it is also interesting to observe that there is a mismatch between the peak electricity demand (orange squares) and the peak electricity generation (dark blue diamonds and light blue crosses). In this case, the batteries installed as part of the system allow the storage of surplus electricity for later use, such that less electricity is exported to the grid during the morning and afternoon (yellow crosses and purple squares), which can then be used in the evening, allowing less electricity to be bought from the grid (grey triangles and green circles). However, some flexibility is still required to import/export electricity from/to the grid, even though FIT are not provided, otherwise a very large battery storage capacity would be required to store the surplus electricity on sunnier days, which would lead to a significantly increased investment cost and system payback time. On the selected winter days, detailed results show that 9% more electricity is exported

Table 8
Utility prices and system economics when all taxes and levies are included of the optimised polymeric flat-box PVT based S-CHP systems in the three locations, with and without financial incentives.

	Prices (€/kWh$_{fe}$)		*PBT* (years)		LPC_{cov} (€/kWh$_{eeq}$)		LPC_{gen} (€/kWh$_{eeq}$)	
	Electricity	Natural Gas	No FIT	FIT	No FIT	FIT	No FIT	FIT
Athens (Greece)	0.1723	0.1020	15.6	12.8†	0.262	0.222†	0.174	0.147†
London (UK)	0.1831	0.0501	22.7	20.4+	0.342	0.324+	0.232	0.220+
Zaragoza (Spain)	0.2284	0.1093	11.6	10.8*	0.293	0.277*	0.200	0.189*

* FIT = 0.048 €/kWh.
\+ FIT = 0.048 €/kWh.
† FIT = 0.105 €/kWh.

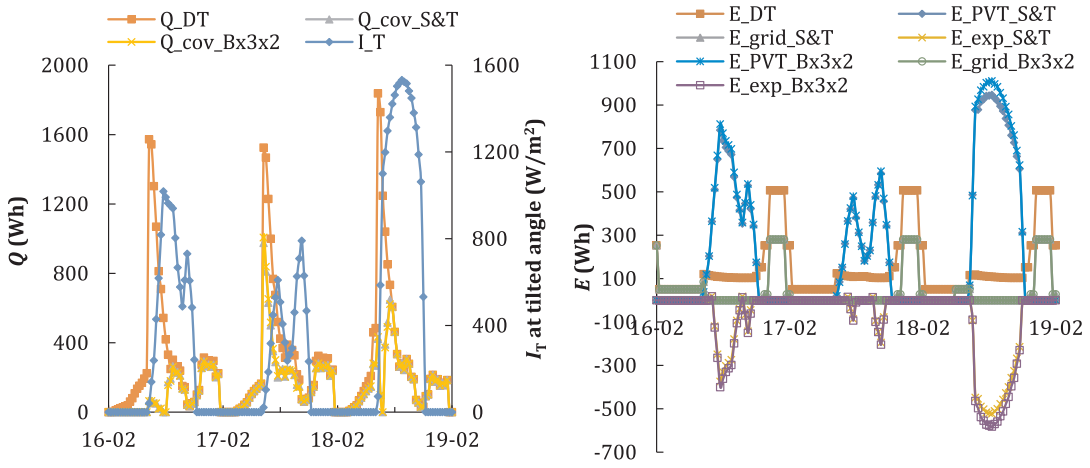

Fig. 10. Optimised S-CHP system operation in Zaragoza (Spain) over three consecutive days in February. (Left) Total solar irradiance at tilted angle (I_T), total household thermal (SH plus DHW) demand (Q_{DT}), thermal demand covered by the optimised PC flat-box PVT ($Q_{cov,B\times3\times2}$) and by the optimised benchmark-PVT ($Q_{cov,S\&T}$) S-CHP systems. (Right) Total household electricity demand (E_{DT}), electricity exported (E_{exp}) and imported (E_{grid}) to/from the grid demand and electricity generated (E_{PVT}) by the optimised PC flat-box PVT (B×3×2) and the optimised benchmark-PVT (S&T) S-CHP systems.

to the grid for the system with the PC 3 × 2 flat-box PVT collectors, compared to the benchmark system with S&T PVT collectors. This is despite the similar amount of the electricity demand covered (around 69%) for both system variants, and is due to the 4% higher amount of electricity generated by the optimised polymeric flat-box PVT collector as a result of its enhanced electrical performance.

Fig. 11 (left) shows time-resolved results over the three consecutive days considered in July. This figure suggests that it is possible to cover almost all (> 99%) of the DHW demand (as there is no SH demand) with both the novel and benchmark PVT systems, despite the lower irradiance on some of the days due to cloud cover. Furthermore, Fig. 11 (right) shows that thanks to the batteries, it is possible to store most of the electricity generated early in the morning when there is low electricity demand, which can be used later in the day to cover an important part of the peak electricity demand occurring in the early evening, due to the cooling electricity consumption required to maintain the internal space comfort temperature at 25 °C [56]. Despite that, some electricity should also be exported to the grid, particularly on days with higher irradiance levels, due to the capacity limitations of the batteries. For the winter case, detailed results show that both systems cover a similar fraction of the household electricity demand (around 68%), however, the system with the optimised polymeric flat-box PVT collectors exports 12% more electricity to the grid.

3.5.2. Optimised S-CHP system in London

For the optimised S-CHP system ($N = 11$ and $V_t = 0.83\,m^3$) installed in London, only the results related to the thermal energy performance in winter (Fig. 12 left), and those corresponding to the electrical performance in summer (Fig. 12 right) are shown in this section, as these are the most relevant results. Equivalent observations to those presented in the previous section can be made for the electrical and thermal performance in winter and summer, respectively.

In Fig. 12 (left), it is possible to observe the differences in the system thermal performance between cloudy and sunny days. The results indicate that on the selected winter days it is only possible to cover around 20% of the entire thermal (DHW plus SH) demand for both the optimised polymeric flat-box PVT-based and benchmark-PVT based S-CHP systems, due to the very low irradiance levels on two of the three days. It is observed that from 12 pm on the first day until 6 am on the second day shown in Fig. 12 (left), all of the thermal demand can be covered thanks to the high irradiance (clear sky day) of the first day which results in a large amount of thermal energy stored in the tank. However, due to the very low irradiance levels of the second day (< 400 W/m² peak), a very limited amount of heat can be extracted

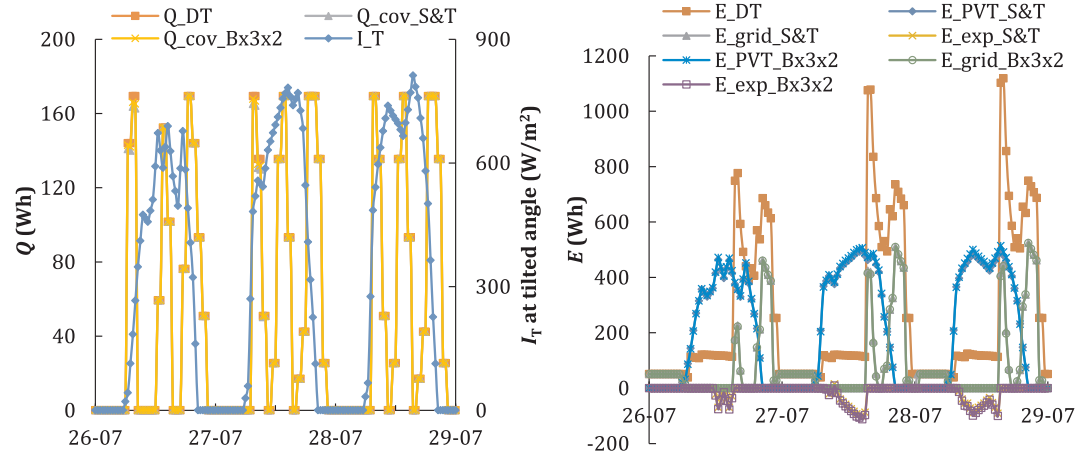

Fig. 11. Optimised S-CHP system operation in Zaragoza (Spain) over three consecutive days in July. (Left) Total solar irradiance at tilted angle (I_T), total household thermal (SH plus DHW) demand (Q_{DT}), thermal demand covered by the optimised PC flat-box PVT ($Q_{cov,B\times3\times2}$) and by the optimised benchmark-PVT ($Q_{cov,S\&T}$) S-CHP systems. (Right) Total household electricity demand (E_{DT}), electricity exported (E_{exp}) and imported (E_{grid}) to/from the grid demand and electricity generated (E_{PVT}) by the optimised PC flat-box PVT (B×3×2) and the optimised benchmark-PVT (S&T) S-CHP systems.

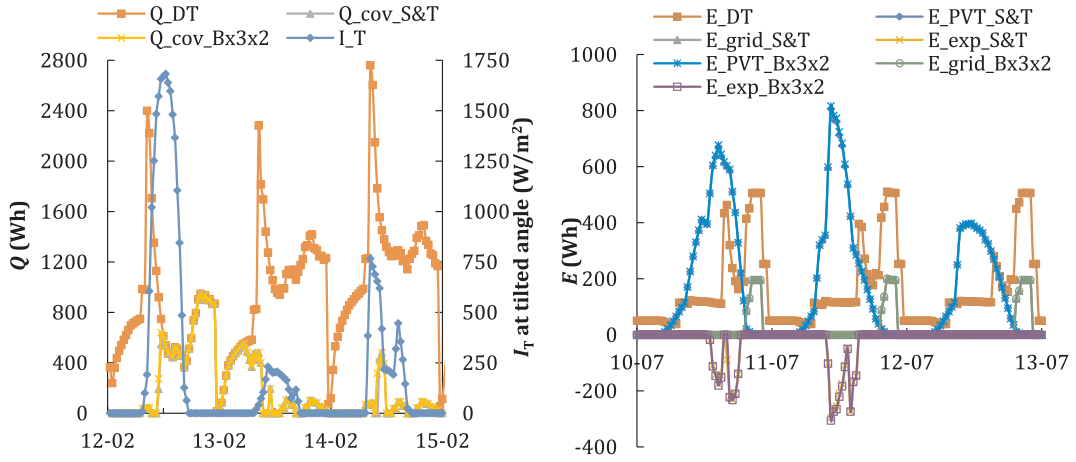

Fig. 12. Optimised S-CHP system operation in London (UK). (Left) Total solar irradiance at tilted angle (I_T), total household thermal (SH plus DHW) demand (Q_{DT}), thermal demand covered by the optimised PC flat-box PVT ($Q_{cov,B\times3\times2}$) and by the optimised benchmark-PVT ($Q_{cov,S\&T}$) S-CHP systems over three consecutive days in February. (Right) Total household electricity demand (E_{DT}), electricity exported (E_{exp}) and imported (E_{grid}) to/from the grid demand and electricity generated (E_{PVT}) by the optimised PC flat-box PVT (B×3×2) and the optimised benchmark-PVT (S&T) S-CHP systems over three consecutive days in July.

from the PVT collectors, which in turn limits the amount of household thermal energy demand that can be covered. Finally, even though the third day has higher irradiance levels than the second, the amount of thermal demand covered is small as the tank temperature has significantly decreased (to around 27–38 °C from bottom to top of the tank) due to the previous day's heat extraction and thermal losses.

The electrical performance results over the three consecutive days in July that were selected for this investigation (see Fig. 12 right) are similar to those generated in Zaragoza. On the first day, the higher electricity generation compared to demand allows the batteries to be charged, so less electricity is exported to the grid. It is observed that only at the end of each day, due to the peak electricity demand for cooling purposes, some electricity should be bought from the grid. Both systems are able to cover 87% of the total electricity demand.

3.5.3. Optimised S-CHP system in Athens

Similarly as before, only the results concerning the thermal energy performance in winter (Fig. 13 left), and those corresponding to the electrical performance in summer (Fig. 13 right) for the S-CHP system ($N = 9$ and $V_t = 0.68\ m^3$) located in Athens are shown.

In Fig. 13 (left), it is possible to observe the differences in the thermal energy performance and operation of both systems between cloudy and sunny days. The results indicate that on the selected winter days it is possible to cover around 70% and 68% of the entire thermal energy (DHW plus SH) demand for both the optimised polymeric flat-box PVT and benchmark-PVT systems respectively. In Fig. 13 (left), it is observed that the thermal demand peak on the first day cannot be covered by the amount of thermal energy stored in the tank (due to lower irradiance levels on the previous day not shown here), but thanks to the high irradiance levels in the middle of the day (the first day is a clear sky day) and the thermal storage capacity of tank, the thermal energy demand is met not only for that afternoon, but also the entire following day and early morning of the third day. However, due to the very low irradiance levels on the third day (peaking at about 400 W/m^2), only a limited amount of the thermal energy demand can be covered after the tank is discharged during the early morning peak.

The electrical performance results on the selected summer days (Fig. 13 right) show that significantly higher electricity generation takes place early in the day (due to the high irradiance levels), in contrast to the lower electricity demand at those times, which allows the batteries to be charged. Later in the day, part of the electricity demand (mainly due to cooling) is then covered by the batteries. In Athens, a key system limitation concerns the storage capacity of the batteries, because even though batteries help to reduce the effect of the

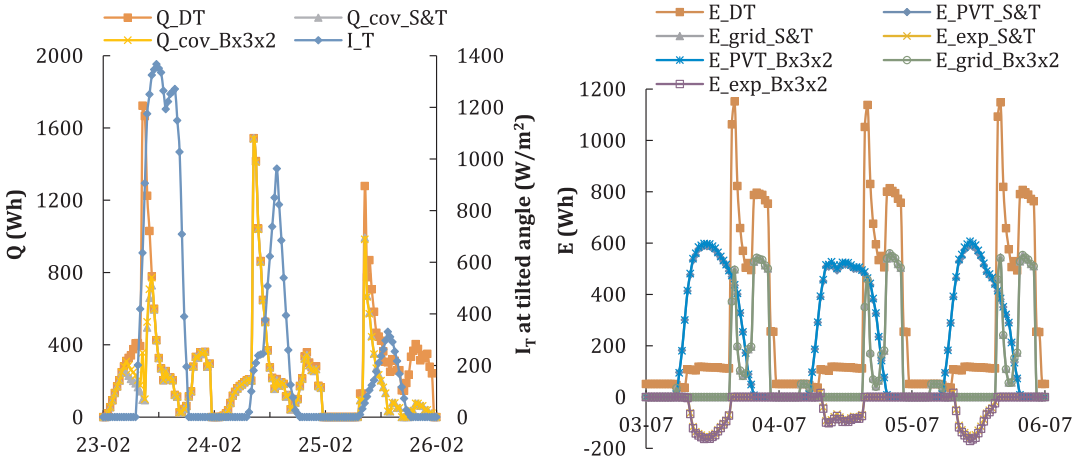

Fig. 13. Optimised S-CHP system operation in Athens (Greece). (Left) Total solar irradiance at tilted angle (I_T), total household thermal (SH plus DHW) demand (Q_{DT}), thermal demand covered by the optimised PC flat-box PVT ($Q_{cov,B\times3\times2}$) and by the optimised benchmark-PVT ($Q_{cov,S\&T}$) S-CHP systems over three consecutive days in February. (Right) Total household electricity demand (E_{DT}), electricity exported (E_{exp}) and imported (E_{grid}) to/from the grid demand and electricity generated (E_{PVT}) by the optimised PC flat-box PVT (B×3×2) and the optimised benchmark-PVT (S&T) S-CHP systems over three consecutive days in July.

mismatch between electricity generation and consumption, not all electricity generated during the day can be stored and later delivered to cover the peak electricity demand in the afternoon and evening. Nevertheless, both system variants are able to cover around 63% of the total electricity demand.

4. Further discussion and conclusions

This paper has been concerned with the technoeconomic performance of solar combined heat and power (S-CHP) systems based on a novel polymeric flat-box PVT collector design proposed and modelled by the authors in previous research [26]. A quasi-steady model of a complete S-CHP system was developed in software EES, comprising a PVT collector array, a water storage tank and a lead-acid electrical battery subsystem. The electrical and thermal energy demands of single-family homes in three different locations (selected to represent a range of regions and climates), namely: Athens (Greece), London (UK) and Zaragoza (Spain) were modelled in EnergyPlus. These energy demand breakdowns along with local weather data, also from EnergyPlus, were used as inputs to the S-CHP system model. The model was run on a half-hourly basis over a carefully selected average week in each month, and key system sizing and operational parameters were assessed and optimised for each month. The monthly results were then used to predict annual performance based on which optimal system size (specifically, the number of PVT collectors and hot-water storage tank size) and operating conditions (specifically, the PVT collector flow-rate) were selected for each location.

An objective of the study was to identify optimal S-CHP systems that minimise payback-time and the associated levelised production cost per kWh of covered household energy. Another objective was to minimise the interaction of these systems with the grid (imported *vs*. exported electricity) and to limit the amount of excess heat rejected to the atmosphere, which is required in order to avoid tank overheating. To meet these objectives, a methodology was developed with which to identify optimal component sizes and also system operating conditions in a systematic way for two S-CHP systems; one based on the novel PVT collectors of interest and one on conventional sheet-and-tube PVT collectors as benchmark case for comparison.

The results show that 9 PVT collectors and a 0.68 m^3 storage tank are recommended for optimal performance in Athens, together with a constant flow-rate through the PVT collector array of 50 L/h. With this configuration, the proposed S-CHP system is capable of covering 64% of the electrical and 61% of the thermal energy demands of the reference house at this location. In London, 11 PVT collectors and a 0.83 m^3 storage tank are recommended, which together with a constant flow-rate of 30 L/h can cover 66% of the electrical and 29% of the thermal energy demands of the reference house. Finally, in Zaragoza, 8 PVT collectors, a 0.72 m^3 storage tank and a constant flow-rate of 65 L/h make it possible to cover 67% of the electrical and 45% of the thermal energy demands of the reference house. It is highlighted that the S-CHP systems based on flat-box collectors outperform their sheet-and-tube equivalents at all studied locations, generating up to 3% more electricity and covering up to 3% more thermal energy demand on an annual basis, at a significantly (21%) lower PVT collector cost.

When considering the economic aspects of the implementation of these S-CHP systems, it is found that in Athens and Zaragoza the proposed systems appear as promising decarbonisation solutions and offer a reasonable-to-attractive payback time (15.6 and 11.6 years respectively), when all taxes and levies are included in the utility prices, even without incentives. Thus, considering a 25-year lifetime, the S-CHP system installations are expected to generate profits for the household for ~10 years in Athens and ~13 years in Zaragoza, thanks to both electricity and fuel-cost savings. In London, due to the low solar irradiance levels and lower ambient temperatures, the estimated system payback time (22.7 years) is closer to the system's lifetime, although this decreases to ~20 years when the FIT currently available in the UK is considered. Therefore, it can be concluded that in order to accelerate the uptake of this technology, which offers a higher (by up to 32%) emission reduction potential compared to PV-only solutions, financial incentives may be required in some regions (e.g. Northern climates), or alternatively the system investment cost should decrease by almost half to make this a cost-effective proposition.

The flat-box PVT-based S-CHP system also outperforms the benchmark equivalent in terms of payback time (9–11% lower) and levelised production cost (4–8% lower) at all studied locations, which can be mainly attributed to the lower cost of the PVT collectors; specifically, 301 € *vs*. 380 €. Furthermore, the optimised S-CHP system also leads to a significant reduction in CO_2 emissions compared to satisfying the household energy demands by conventional means. The high carbon emission factor of the electricity grid in Greece makes these systems particularly promising at this location. Specifically, potential savings of 3.87 tons CO_2 over a year in Athens, 1.54 tons CO_2/year in London and 1.65 tons CO_2/year in Zaragoza were identified. By comparison, PV-only solutions displace 3.56, 1.21, 1.22 tCO_2/year for the same area and 10.85, 3.41, 3.98 tCO_2/year for the same cost, but with installed PV-covered surface areas of 43, 49 and 41 m^2, respectively.

This technoeconomic analysis shows that the geographical location and climate have a significant effect on the performance and cost-effectiveness of the proposed S-CHP system, with low irradiance conditions resulting in a higher demand for auxiliary heat and higher fuel costs, and high irradiance conditions resulting in a lower demand for auxiliary heat but also a higher electricity demand, particularly in the summer for cooling purposes. Beyond the potential energy generated (and demand covered) by the S-CHP system, the results show that these type of systems, whose payback time depends on the achievable fuel savings, are particularly sensitive to utility prices, specific to each location. A clear example of this observation arises in the case of Athens, where, despite the potential of the proposed S-CHP system to cover ~65% of the electrical and ~62% of the thermal energy demands, the system payback time is higher than that of Zaragoza, where a lower fraction of thermal demand is covered but utility prices are higher.

Finally, it is noted that the costs of the various S-CHP system components considered in the present work were obtained from current European retailers, except for the novel PVT collector, which was estimated from raw material prices and production costs. Thus, a further reduction of these costs, especially the collector manufacturing costs, can be expected with the widespread uptake of the technology. Further, an increase in the price of fossil fuels, amongst other factors, is expected to lead to higher utility prices, which can act to decrease further the payback times of the proposed S-CHP systems from those reported here.

Acknowledgements

This work was supported by the UK Engineering and Physical Sciences Research Council (EPSRC) [grant number EP/M025012/1]. The technical specifications of the commercially available ECOMESH panel were provided by the PVT collector manufacturer, EndeF Engineering. Data supporting this publication can be obtained on request from cep-lab@imperial.ac.uk.

References

[1] Markides CN. The role of pumped and waste heat technologies in a high-efficiency sustainable energy future for the UK. Appl Therm Eng 2013;53(2):197–209. https://doi.org/10.1016/j.applthermaleng.2012.02.037.

[2] Markides CN. Low-concentration solar-power systems based on organic Rankine cycles for distributed-scale applications: Overview and further developments. Front Energy Res 2015;3(47):1–16. https://doi.org/10.3389/fenrg.2015.00047.

[3] Makki A, Omer S, Sabir H. Advancements in hybrid photovoltaic systems for enhanced solar cells performance. Renew Sustain Energy Rev 2015;41:658–84. https://doi.org/10.1016/j.rser.2014.08.069.

[4] Ramos A, Guarracino I, Mellor A, Alonso-Álvarez D, Childs P, Ekins-Daukes NJ, et al. Solar-thermal and hybrid photovoltaic-thermal systems for renewable heating Briefing Paper 22 Grantham Institute, Imperial College London; 2017. p. 1–19.

https://www.imperial.ac.uk/media/imperial-college/grantham-institute/public/publications/briefing-papers/2679_Briefing-P-22-Solar-heat_web.pdf.
[5] Ramos A, Chatzopoulou MA, Guarracino I, Freeman J, Markides CN. Hybrid photovoltaic-thermal solar systems for combined heating, cooling and power provision in the urban environment. Energy Convers Manag 2017;150:838–50. https://doi.org/10.1016/j.enconman.2017.03.024.
[6] Bakos G, Soursos M, Tsagas N. Technoeconomic assessment of a building-integrated PV system for electrical energy saving in residential sector. Energy Build 2003;35:757–62. https://doi.org/10.1016/S0378-7788(02)00229-3.
[7] Hoppmann J, Volland J, Schmidt TS, Hoffmann VH. The economic viability of battery storage for residential solar photovoltaic systems – A review and a simulation model. Renew Sustain Energy Rev 2014;39:1101–18. https://doi.org/10.1016/j.rser.2014.07.068.
[8] Romero Rodríguez L, Salmerón Lissén JM, Sánchez Ramos J, Rodríguez Jara EÁ, Álvarez Domínguez S. Analysis of the economic feasibility and reduction of a building's energy consumption and emissions when integrating hybrid solar thermal/PV/micro-CHP systems. Appl Energy 2016;165:828–38. https://doi.org/10.1016/j.apenergy.2015.12.080.
[9] Freeman J, Hellgardt K, Markides CN. An assessment of solar-powered organic Rankine cycle systems for combined heating and power in UK domestic applications. Appl Energy 2015;138:605–20. https://doi.org/10.1016/j.apenergy.2014.10.035.
[10] Freeman J, Hellgardt K, Markides CN. Working fluid selection and electrical performance optimisation of a domestic solar-ORC combined heat and power system for year-round operation in the UK. Appl Energy 2017;186:291–303. https://doi.org/10.1016/j.apenergy.2016.04.041.
[11] Freeman J, Guarracino I, Kalogirou SA, Markides CN. A small-scale solar organic Rankine cycle combined heat and power system with integrated thermal energy storage. Appl Therm Eng 2017;127:1543–54. https://doi.org/10.1016/j.applthermaleng.2017.07.163.
[12] Ramos A, Chatzopoulou MA, Freeman J, Markides CN. Optimisation of a high-efficiency solar-driven organic Rankine cycle for applications in the built environment. Appl Energy 2018;228:755–65. https://doi.org/10.1016/j.apenergy.2018.06.059.
[13] Modi A, Bühler F, Andreasen JG, Haglind F. A review of solar energy based heat and power generation systems. Renew Sustain Energy Rev 2017;67:1047–64. https://doi.org/10.1016/j.rser.2016.09.075.
[14] Chow TT, Ji J, He W. Photovoltaic-thermal collector system for domestic application. J Sol Energy Eng 2007;129:205. https://doi.org/10.1115/1.2711474.
[15] Affolter P, Eisenmann W, Fechner H, Rommel M, Schaap A, Sorensen H, et al. PVT roadmap: A European guide for the development and market introduction of PV-Thermal technology. Proceedings of: 20th European Photovoltaic Solar Energy Conference (EU PVSEC). 2005.
[16] Zondag HA, de Vries DW, van Helden WGJ, van Zolingen RJC, van Steenhoven AA. The yield of different combined PV-thermal collector designs. Sol Energy 2003;74:253–69. https://doi.org/10.1016/S0038-092X(03)00121-X.
[17] Chow TT. Performance analysis of photovoltaic-thermal collector by explicit dynamic model. Sol Energy 2003;75:143–52. https://doi.org/10.1016/j.solener.2003.07.001.
[18] Kalogirou SA. Use of TRNSYS for modelling and simulation of a hybrid PV–thermal solar system for Cyprus. Renew Energy 2001;23:247–60. https://doi.org/10.1016/S0960-1481(00)00176-2.
[19] Herrando M, Markides CN, Hellgardt K. A UK-based assessment of hybrid PV and solar-thermal systems for domestic heating and power: System performance. Appl Energy 2014;122:288–309. https://doi.org/10.1016/j.apenergy.2014.01.061.
[20] He W, Chow T, Ji J, Lu J, Pei G. Hybrid photovoltaic and thermal solar-collector designed for natural circulation of water. Appl Energy 2006;83:199–210. https://doi.org/10.1016/j.apenergy.2005.02.007.
[21] Huang BJ, Lin TH, Hung WC, Sun FS. Performance evaluation of solar photovoltaic/thermal systems. Sol Energy 2001;70:443–8.
[22] Shan F, Cao L, Fang G. Dynamic performances modeling of a photovoltaic-thermal collector with water heating in buildings. Energy Build 2013;66:485–94. https://doi.org/10.1016/j.enbuild.2013.07.067.
[23] Cristofari C, Canaletti J, Notton G, Darras C. Innovative patented PV/TH solar collector: Optimization and performance evaluation. Energy Procedia 2012;14:235–40.
[24] Cristofari C, Notton G, Poggi P, Louche A. Modelling and performance of a copolymer solar water heating collector. Sol Energy 2002;72:99–112. https://doi.org/10.1016/S0038-092X(01)00092-5.
[25] Chow TT, He W, Ji J. Hybrid photovoltaic-thermosyphon water heating system for residential application. Sol Energy 2006;80:298–306. https://doi.org/10.1016/j.solener.2005.02.003.
[26] Herrando M, Guarracino I, del Amo A, Zabalza I, Markides CN. Energy characterization and optimization of new heat recovery configurations in hybrid PVT systems. Proceedings of: 11th International Conference on Solar Energy for Buildings and Industry (EuroSun) 2016. https://doi.org/10.18086/eurosun.2016.08.22.
[27] Kalogirou SA, Tripanagnostopoulos Y. Hybrid PV/T solar systems for domestic hot water and electricity production. Energy Convers Manag 2006;47:3368–82. https://doi.org/10.1016/j.enconman.2006.01.012.
[28] Kalogirou SA, Tripanagnostopoulos Y. Industrial application of PV/T solar energy systems. Appl Therm Eng 2007;27:1259–70. https://doi.org/10.1016/j.applthermaleng.2006.11.003.
[29] Tripanagnostopoulos Y, Souliotis M, Battisti R, Corrado A. Energy, cost and LCA results of PV and hybrid PV/T solar systems. Prog Photovolt Res Appl 2005;13:235–50. https://doi.org/10.1002/pip.590.
[30] Tselepis S, Tripanagnostopoulos Y. Ecomomic analysis of hybrid photovoltaic/thermal solar systems and comparison with standard PV modules, PV in Europe – From PV technology to energy solutions; 2002.
[31] Zhang X, Zhao X, Smith S, Xu J, Yu X. Review of R&D progress and practical application of the solar photovoltaic/thermal (PV/T) technologies. Renew Sustain Energy Rev 2012;16:599–617. https://doi.org/10.1016/j.rser.2011.08.026.
[32] Bagge H, Johansson D. Measurements of household electricity and domestic hot water use in dwellings and the effect of different monitoring time resolution. Energy 2011;36:2943–51. https://doi.org/10.1016/j.energy.2011.02.037.
[33] Vokas G, Christandonis N, Skittides F. Hybrid photovoltaic – thermal systems for domestic heating and cooling—a theoretical approach. Sol Energy 2006;80:607–15. https://doi.org/10.1016/j.solener.2005.03.011.
[34] Chow TT, Chan ALS, Fong KF, Lin Z, He W, Ji J. Annual performance of building-integrated photovoltaic/water-heating system for warm climate application. Appl Energy 2009;86:689–96. https://doi.org/10.1016/j.apenergy.2008.09.014.
[35] Calise F, Dentice D'Accadia M, Vanoli L. Design and dynamic simulation of a novel solar trigeneration system based on hybrid photovoltaic/thermal collectors (PVT). Energy Convers Manag 2012;60:214–25. https://doi.org/10.1016/j.enconman.2012.01.025.
[36] Calise F, Figaj RD, Vanoli L. A novel polygeneration system integrating photovoltaic/thermal collectors, solar assisted heat pump, adsorption chiller and electrical energy storage: Dynamic and energy-economic analysis. Energy Convers Manag 2017;149:798–814. https://doi.org/10.1016/j.enconman.2017.03.027.
[37] EnergyPlus. EnergyPlus software; 2017.
[38] Cristofari C, Notton G, Canaletti JL. Thermal behavior of a copolymer PV/Th solar system in low flow rate conditions. Sol Energy 2009;83:1123–38. https://doi.org/10.1016/j.solener.2009.01.008.
[39] Hobbi A, Siddiqui K. Optimal design of a forced circulation solar water heating system for a residential unit in cold climate using TRNSYS. Sol Energy 2009;83:700–14. https://doi.org/10.1016/j.solener.2008.10.018.
[40] Luthander R, Widen J, Nilsson D, Palm J. Photovoltaic self-consumption in buildings: A review. Appl Energy 2015;142:80–94. https://doi.org/10.1016/j.apenergy.2014.12.028.
[41] Freeman J, Hellgardt K, Markides CN. An assessment of solar–thermal collector designs for small-scale combined heating and power applications in the United Kingdom. Heat Transf Eng 2015;36(14–15):1332–47. https://doi.org/10.1080/01457632.2015.995037.
[42] European Commission. Best practices on Renewable Energy Self-consumption. Brussels; 2015.
[43] Parra D, Walker GS, Gillott M. Modeling of PV generation, battery and hydrogen storage to investigate the benefits of energy storage for single dwelling. Sustain Cities Soc 2014;10:1–10. 10.1016/j.scs.2013.04.006.
[44] Mahmoud MM. On the storage batteries used in solar electric power systems and development of an algorithm for determining their ampere-hour capacity. Electr Power Syst Res 2004;71:85–9. https://doi.org/10.1016/j.epsr.2003.12.018.
[45] F-Chart. EES Engineering Equation Solver | F-Chart Software, Engineering Software; 2017.
[46] Herrando M, Freeman J, Ramos A, Zabalza I, Markides CN. Energetic and economic optimisation of a novel hybrid PV-thermal system for domestic combined heating and power. Proceedings of: 13th International Conference on Heat Transfer, Fluid Mechanics and Thermodynamics (HEFAT). 2017.
[47] Agarwal RK, Garg HP. Study of a photovoltaic-thermal system - thermosyphonic solar water heater combined with solar cells. Energy Convers Manag 1994;35:605–20.
[48] Notton G, Cristofari C, Mattei M, Poggi P. Modelling of a double-glass photovoltaic module using finite differences. Appl Therm Eng 2005;25:2854–77. https://doi.org/10.1016/j.applthermaleng.2005.02.008.
[49] Tiwari A, Sodha MS. Performance evaluation of solar PV/T system: An experimental validation. Sol Energy 2006;80:751–9. https://doi.org/10.1016/j.solener.2005.07.006.
[50] Bhattarai S, Oh J, Euh S, Krishna G, Hyun D. Simulation and model validation of sheet and tube type photovoltaic thermal solar system and conventional solar collecting system in transient states. Sol Energy Mater Sol Cells 2012;103:184–93. https://doi.org/10.1016/j.solmat.2012.04.017.
[51] Sandnes B, Rekstad J. A photovoltaic/thermal (PV/T) collector with a polymer absorber plate. Experimental study and analytical model. Sol Energy 2002;72:63–73. https://doi.org/10.1016/S0038-092X(01)00091-3.
[52] Zondag HA, De Vries DW, Van Helden WGJ, Van Zolingen RJC, van Steenhoven AA. The thermal and electrical yield of a PV-thermal collector. Sol Energy 2002;72:113–28. https://doi.org/10.1016/S0038-092X(01)00094-9.
[53] EndeF Engineering. Technical Datasheet ECOMESH panel, 2015.
[54] Kalogirou SA. Solar thermal collectors and applications. Prog Energy Combust Sci 2004;30:231–95. https://doi.org/10.1016/j.pecs.2004.02.001.
[55] ASHRAE Standard. Standard 93-2003: Methods of testing to determine the performance of solar collectors; 2013.
[56] Gobierno de España. Orden FOM/1635/2013, de 10 de septiembre, por la que se actualiza el Documento Básico DB-HE «Ahorro de Energía», del Código Técnico de la Edificación, aprobado por Real Decreto 314/2006, de 17 de marzo; 2013.
[57] IDAE and CENSOLAR. Solar thermal energy installations. Technical specifications document of low temperature installations; 2009.
[58] Drück H. MULTIPORT store – Model for TRNSYS; 2006.
[59] Lunde PJ. Solar thermal engineering: Space heating and hot water systems. John Wiley and Sons; 1980.
[60] Incropera FP, DeWitt DP, Bergman TL, Lavine AS. Fundamentals of heat and mass transfer. 6th ed. John Wiley and Sons; 2007.
[61] Cruickshank CA, Harrison SJ. Heat loss characteristics for a typical solar domestic hot water storage. Energy Build 2010;42:1703–10. https://doi.org/10.1016/j.

enbuild.2010.04.013.
[62] Kreith F, Goswami DY. Handbook of energy efficiency and renewable energy. CRC Press; 2007.
[63] Daikin. Product groups | Daikin, www.daikin.co.uk/en_gb/product-group.html [accessed 29.06.17].
[64] Badescu V. Optimal control of flow in solar collector systems with fully mixed water storage tanks. Energy Convers Manag 2008;49:169–84. https://doi.org/10.1016/j.enconman.2007.06.022.
[65] Guarracino I, Mellor A, Ekins-Daukes NJ, Markides CN. Dynamic coupled thermal-and-electrical modelling of sheet-and-tube hybrid photovoltaic/thermal (PVT) collectors. Appl Therm Eng 2016;101:778–95. https://doi.org/10.1016/j.applthermaleng.2016.02.056.
[66] Knudsen S. Consumers' influence on the thermal performance of small SDHW systems - Theoretical investigations. Sol Energy 2002;73:33–42. https://doi.org/10.1016/S0038-092X(02)00018-X.
[67] Beckman WA, Thornton J, Long S, Wood BD. Control problems in solar domestic hot water systems. Sol Energy 1994;53:233–6. https://doi.org/10.1016/0038-092X(94)90629-7.
[68] White FM. Fluid mechanics. 6th ed. McGraw-Hill; 2008.
[69] International Renewable Energy Agency (IRENA). Off-grid, PV power systems – System design guidelines; 2012.
[70] Ghafoor A, Munir A. Design and economics analysis of an off-grid PV system for household electrification. Renew Sustain Energy Rev 2015;42:496–502. https://doi.org/10.1016/j.rser.2014.10.012.
[71] Akikur RK, Saidur R, Ping HW, Ullah KR. Comparative study of stand-alone and hybrid solar energy systems suitable for off-grid rural electrification: A review. Renew Sustain Energy Rev 2013;27:738–52. https://doi.org/10.1016/j.rser.2013.06.043.
[72] World Meteorological Organization. World Meteorological Organization Extranet, www.wmo.int/pages/index_es.html [accessed 13.08.17].
[73] Duffie JA, Beckman WA, Worek WM. Solar engineering of thermal processes. John Wiley and Sons; 1974. https://doi.org/10.1115/1.2930068.
[74] JRC European Commission. Photovoltaic geographical information system – PV potential estimation utility, re.jrc.ec.europa.eu/pvgis/apps4/pvest.php [accessed 27.11.17].
[75] Hansen J, Sorensen H. IEA SHC task 35 PV/thermal solar systems. IEA 2006.
[76] International Energy Agency (IEA). Technology roadmap: Solar photovoltaic energy. 2010. https://doi.org/10.1787/9789264088047-en.
[77] Herrando M, Markides CN. Hybrid PV and solar-thermal systems for domestic heat and power provision in the UK: Techno-economic considerations. Appl Energy 2016;161:512–32. https://doi.org/10.1016/j.apenergy.2015.09.025.
[78] EndeF Engineering. Endef – Energy, Development and future; 2017.
[79] Barilla Solar. Wholesale solar thermal supplies barilla solar. http://www.barillasolar.co.uk [accessed 19.07.17].
[80] Navitron. http://www.navitron.org.uk [accessed 19.07.17].
[81] PV Direct. Wholesale solar panels | Solar PV | Photovoltaic panels | BuyPVDirect UK's largest PV manufacturer and distributor. http://www.buypvdirect.co.uk [accessed 19.07.17].
[82] Viridian Solar. The pod – Solar water heating simplified. http://www.viridiansolar.co.uk/solar-products-solar-heating-with-combi-pod.html [accessed 19.07.17].
[83] Lapesa. GEISER INOX | lapesa. http://www.lapesa.es/en/domestic-hot-water/geiser-inox.html [accessed 19.07.17].
[84] Wagner Renewable. Home page – Wagner renewables. http://www.wagnersolarshop.com [accessed 19.07.17].
[85] Autosolar. Batería 70Ah 12V UPower SPO70 | al mejor precio. http://www.autosolar.es/bateria-12v/bateria-70ah-12v-upower-spo70 [accessed 09.06.17].
[86] Eurostat. Database – Energy statistics – Prices; 2017.
[87] BRE. SAP 2012. The Government's standard assessment procedure for energy rating of dwellings. 2014. https://doi.org/10.1007/s13398-014-0173-7.2.
[88] Herrando M, Ramos A, Zabalza I. Cost competitiveness of a novel PVT-based solar combined heating and power system: Influence of economic parameters and financial incentives. Energy Convers Manag 2018;166:758–70. https://doi.org/10.1016/j.enconman.2018.04.005.
[89] KPMG. UK solar beyond subsidy: The transition; 2015.
[90] RES Legal. Feed-in tariff II (rooftop PV) in Greece 2017. http://www.res-legal.eu/search-by-country/greece/single/s/res-e/t/promotion/aid/feed-in-tariff-ii-pv-on-rooftops/lastp/139 [accessed 18 July 2017].
[91] Department for Business Energy & Industrial Strategy – UK Government. 2016 Government GHG conversion factors for company reporting, Methodology paper for emission factors; 2016.
[92] Gobierno de España. Factores de emisión de CO_2 y coeficientes de paso a energía primaria de diferentes fuentes de energía final consumidas en el sector de edificios en España; 2016.
[93] Greek Government. Conversion factors in Greece; 2012.
[94] HM Treasury – Public Service Transformation Network. Supporting public service transformation: Cost benefit analysis guidance for local partnerships; 2014.
[95] Tucker J. Consumer prices inflation (CPI) time series dataset. Office for National Statistics, UK Government; 2018.
[96] inflation.eu. Historic inflation – Overview of CPI inflation year. Worldwide inflation data 2017. http://www.inflation.eu/inflation-rates/historic-cpi-inflation.aspx [accessed 05.03.18].
[97] Kim Y, Thu K, Kaur H, Singh C, Choon K. Thermal analysis and performance optimization of a solar hot water plant with economic evaluation. Sol Energy 2012;86:1378–95. https://doi.org/10.1016/j.solener.2012.01.030.